Nonlin. Processes Geophys., 21, 303–323, 2014
www.nonlin-processes-geophys.net/21/303/2014/
doi:10.5194/npg-21-303-2014

Nonlinear Processes in Geophysics
Open Access

A hybrid variational ensemble data assimilation for the HIgh Resolution Limited Area Model (HIRLAM)

N. Gustafsson[1], **J. Bojarova**[2], **and O. Vignes**[2]

[1]Swedish Meteorological and Hydrological Institute, 60176 Norrköping, Sweden
[2]Norwegian Meteorological Institute, P.O. Box 43 Blindern, 0313 Oslo, Norway

Correspondence to: N. Gustafsson (nils.gustafsson@smhi.se)

Received: 7 May 2013 – Revised: 19 January 2014 – Accepted: 26 January 2014 – Published: 26 February 2014

Abstract. A hybrid variational ensemble data assimilation has been developed on top of the HIRLAM variational data assimilation. It provides the possibility of applying a flow-dependent background error covariance model during the data assimilation at the same time as full rank characteristics of the variational data assimilation are preserved. The hybrid formulation is based on an augmentation of the assimilation control variable with localised weights to be assigned to a set of ensemble member perturbations (deviations from the ensemble mean). The flow-dependency of the hybrid assimilation is demonstrated in single simulated observation impact studies and the improved performance of the hybrid assimilation in comparison with pure 3-dimensional variational as well as pure ensemble assimilation is also proven in real observation assimilation experiments. The performance of the hybrid assimilation is comparable to the performance of the 4-dimensional variational data assimilation. The sensitivity to various parameters of the hybrid assimilation scheme and the sensitivity to the applied ensemble generation techniques are also examined. In particular, the inclusion of ensemble perturbations with a lagged validity time has been examined with encouraging results.

1 Introduction

Data assimilation is the process of utilising meteorological observations to determine the initial state for Numerical Weather Prediction (NWP) models. Early during the development of NWP it was realised that statistical estimation methods could be utilised in the data assimilation process (Gandin, 1963) and data assimilation research has mainly been focused on statistical estimation methods since then. Since the dimension of the NWP model state is of order 10^7–10^9 and several orders of magnitude larger than the number of available observations at any particular moment in time (10^5–10^6), it is necessary to take prior information into account. A short range forecast, which includes the influence of the time-history of observations, is often taken as the prior estimate of the model state and is generally called the *background* state. The error covariance of the background state is used to characterise the background state uncertainty. One can say that assumptions about Gaussianity lies behind this approach.

A core issue in the development of data assimilation algorithms for NWP has been the formulation of models for the background error covariance. Development started with time independent (climatological) horizontal background error correlation models being essentially functions of horizontal distance separation only (Gandin, 1963). The background error correlation models of these techniques, also known as Optimum Interpolation (OI) or statistical interpolation techniques, were later on generalised to become 3-D by including the vertical direction and also by including multi-variate balance constraints like the geostrophic balance (Lorenc, 1981). Most implementations of statistical interpolation have in common that the background error covariance has a static (climatological) formulation, with the effect that the weights given to the observations are independent of the actual flow situation and also independent of the information content of previously assimilated observations.

The Kalman filter (Kalman, 1960) provides a framework for estimation of the mean and the covariance of the model state for linear forecast models and the extended Kalman (Kalman and Bucy, 1961) filter provides an extension of the Kalman filter to weakly nonlinear forecast models. In

combination with the Kalman Smoother recursions (Durbin and Koopman, 1997) Kalman filtering can be extended to the non-Gaussian and nonlinear frameworks. Due to the large dimension of the model state vector of NWP models, the Extended Kalman filter and the Kalman smoother are not directly possible to apply for full-scale meteorological data assimilation problems. There exist, however, several approximations to the Extended Kalman filter and the Kalman smoother that are possible to utilise also for full-scale meteorological data assimilation. 4D-Var, and in particular the incremental 4D-Var (Courtier et al., 1994), can be viewed as a practical solution to the Kalman smoother over a limited assimilation time window. One weakness of the 4D-Var approximation to the Kalman smoother can be the application of a climatological background error covariance at the start of each assimilation window, although this can be alleviated in several ways (Fisher, 2003). This particular weakness of 4D-Var is overcome with various versions of Ensemble Kalman filters and smoothers (EnKF, Evensen, 1994, 2007). With a limited number of ensemble members, which is always the case for any full-scale ensemble data assimilation problem, the EnKF, however, suffers from a severe rank deficiency.

The current two main streams in development of meteorological data assimilation are the 4D-Var and the EnKF. Advantages and disadvantages of these two approaches to data assimilation were discussed by Kalnay et al. (2007) and Gustafsson (2007). The consensus of this discussion is the necessity to form a synthesis of the two approaches to meteorological data assimilation. Such a synthesis, a Hybrid Variational Ensemble data assimilation for the HIRLAM (HIgh Resolution Limited Area Model) forecasting system (Undén et al., 2002) is the subject of the present study.

Hybrid variational ensemble data assimilation algorithms are described and discussed in Sect. 2, followed by a brief overview of the HIRLAM variational data assimilation in Sect. 3 and by a description of the implementation of the hybrid assimilation algorithm into the HIRLAM variational data assimilation in Sect. 4. For the generation of ensemble perturbations we apply two techniques, the Ensemble Transform Kalman Filter (ETKF) re-scaling technique (Bishop et al., 2001) and the Ensemble of Data Assimilations (EDA) technique (Houtekamer et al., 1996; Fisher, 2003) based on perturbation of data assimilation input data (observations and background). These techniques are described in Sect. 5. Results from data assimilation experiments for one shorter summer period and one longer winter period are provided in Sect. 6. We compare the impact of the ensemble generation technique on the quality of the hybrid assimilation and we examine the sensitivity of the hybrid assimilation scheme to various parameters. Some concluding remarks are given in Sect. 7.

2 Formulations of hybrid variational ensemble data assimilation algorithms

Hybrid variational ensemble data assimilation algorithms aim to combine the advantages of the full rank error covariance matrices of variational algorithms with the advantages of the flow-dependency of the covariances of ensemble data assimilation algorithms, for example, Ensemble Kalman Filters (EnKF). There are also strong efforts currently to develop hybrids of ensemble data assimilation algorithms and Particle Filter (PF) algorithms (van Leeuwen, 2009), in order to better handle the nonlinearities of the forecast models and the observation operators (Papadakis et al., 2010). These developments, including PF ideas, have not yet reached a mature stage enough to be applied to full-scale numerical weather prediction problems.

Essentially there have been two approaches to combine variational data assimilation techniques with ensemble data assimilation techniques. One approach is to compute an heterogeneous covariance model in a flow-dependent way, for instance by using ensemble data to derive spatially and temporally variable background error variances (Fisher, 2003; Berre and Desroziers, 2010). A further step in this direction is to represent background error correlations by, for example, flow-dependent correlation models based on wavelet formulations (Pannekoucke et al., 2007). The second approach is to utilise the original (raw) ensemble covariances in linear combinations with full rank variational covariance models, possibly also applying localisation techniques to the ensemble component (Hamill and Snyder, 2000; Lorenc, 2003; Buehner, 2005). These techniques will be described in more detail below. One particular and promising line of development within this approach is also to replace the integration of the tangent linear and adjoint models in 4D-Var with a 4-D ensemble of nonlinear forecast model states over the assimilation window (4DEnVar, Liu et al., 2008, 2009; Buehner et al., 2010a, b).

Hamill and Snyder (2000) suggest that the background error covariance $\mathbf{B}$ of the hybrid variational ensemble data assimilation technique should be formed as a linear combination of a climatological 3D-Var based covariance $\mathbf{B}_{\text{var}}$ and a flow-dependent ensemble-based covariance $\mathbf{B}_{\text{ens}}$:

$$\mathbf{B} = w_{\text{var}}\mathbf{B}_{\text{var}} + w_{\text{ens}}\mathbf{B}_{\text{ens}} \quad (1)$$

with the following constraint on the weight w_{var} for the climatological part of the covariance and the weight w_{ens} for the ensemble part of the covariance

$$w_{\text{var}} + w_{\text{ens}} = 1 \quad (2)$$

in order to preserve the total background error variance in the case it is similar in $\mathbf{B}_{\text{var}}$ and in $\mathbf{B}_{\text{ens}}$. As is the case with any Ensemble Kalman Filter background error covariance in physical space, the utilisation of a relatively small number of ensemble members will result in poorly estimated small

correlations, for example, those at relatively large horizontal distance separations. If not handled properly, these poorly estimated small correlations may result in spurious correlations, and the corresponding spurious influence of observations at large distance separations. In order to minimise the adverse effects of such poorly estimated small correlations, one may introduce a localised Ensemble Kalman filter (Ott et al., 2004) or one may modify the raw ensemble based covariances to asymptotically approach zero at large distance separations. One way to achieve this is via an element-by-element multiplication of the raw ensemble covariance matrix $\mathbf{B}_{\text{raw-ens}}$ with another correlation matrix $\mathbf{A}$ based on a correlation model for which the correlations approach zero at large distance separations (a so called Schur product, here denoted by $\circ$).

$$\mathbf{B}_{\text{ens}} = \mathbf{A} \circ \mathbf{B}_{\text{raw-ens}} \tag{3}$$

The suggested hybrid variational ensemble data assimilation by Hamill and Snyder (2000) is relatively easy to implement in case the optimisation for the assimilation weights is carried out in observation space. In most operationally applied variational data assimilation schemes, however, the optimisation is carried out in model space via a minimisation of a cost function that depends on the assimilation increment in model space. Thus, the covariance matrix to be inverted has the dimension of the model state vector, and this huge dimension prohibits a direct inversion of the covariance matrix. In this case the minimisation problem is generally solved iteratively and the minimisation problem is pre-conditioned via simplifying assumptions about the background error covariance.

Lorenc (2003) suggested an alternative hybrid variational ensemble data assimilation algorithm that solves the minimisation problem by an augmentation of the assimilation control vector and by adding an additional cost function term, which represents the weights given to the different ensemble members. Thus, the total assimilation increment $\delta\boldsymbol{x}$ can be considered to include two parts, one part $\delta\boldsymbol{x}_{\text{var}}$ corresponding to the constraint given by the climatological background error covariance, and another part that is a linear combination, with space-dependent weights, of the ensemble perturbations, i.e. the deviations between the ensemble members and the ensemble mean:

$$\delta\boldsymbol{x} = \delta\boldsymbol{x}_{\text{var}} + \kappa \sum_{k=1}^{K} \left(\boldsymbol{\alpha}_k \circ \delta\boldsymbol{x}_k^{\text{ens}}\right) \tag{4}$$

where K is the number of ensemble members, κ is a tuning factor, $\boldsymbol{\alpha}_k$ is the vector of weights given to ensemble member k in the linear combination of ensemble perturbations and

$$\delta\boldsymbol{x}_k^{\text{ens}} = \boldsymbol{x}_k^{\text{ens}} - \overline{\boldsymbol{x}^{\text{ens}}} \tag{5}$$

is the ensemble perturbation, i.e. the deviation of the kth background ensemble member from the ensemble mean. The weights given to the ensemble background perturbations may be functions of horizontal and vertical position and these weights are determined by adding an ensemble constraint $J_{\text{ens}}(\boldsymbol{\alpha})$, being a function of the matrix $\boldsymbol{\alpha}$ of all the weights for the different ensemble members, to the cost function to be minimised. Thus, in the case of a hybrid variational ensemble data assimilation, we will have for the total cost function

$$J\left(\delta\boldsymbol{x}_{\text{var}}, \boldsymbol{\alpha}\right) = \beta_{\text{var}} J_{\text{var}}\left(\delta\boldsymbol{x}_{\text{var}}\right) + \beta_{\text{ens}} J_{\text{ens}}(\boldsymbol{\alpha}) + J_{\text{o}} \tag{6}$$

where $J_{\text{var}}(\delta\boldsymbol{x}_{\text{var}})$ denotes the original variational background error constraint, based on a climatological background error covariance, and J_{o} the original variational observation error constraint.

In order to preserve the total background error variance in the case it is similar in $\mathbf{B}_{\text{var}}$ and in $\mathbf{B}_{\text{ens}}$, the weights for the two parts of the background error cost-function terms need to fulfil

$$\frac{1}{\beta_{\text{var}}} + \frac{1}{\beta_{\text{ens}}} = 1. \tag{7}$$

The ensemble background error cost function can be formulated in the following way

$$J_{\text{ens}} = \frac{1}{2}\boldsymbol{\alpha}^T \mathbf{A}^{-1}\boldsymbol{\alpha} \tag{8}$$

where the covariance matrix $\mathbf{A}$ can be interpreted as a covariance for the localised ensemble member weights described by, for example, a variance and a spatial scale of the localised ensemble weights. In the expressions above $\boldsymbol{\alpha}_k \circ \delta\boldsymbol{x}_k^{\text{ens}}$ means element-by-element multiplication. Wang et al. (2007) have proven that the two formulations of the hybrid variational ensemble data assimilation are equivalent.

The main advantage of the version of the hybrid method proposed by Lorenc (2003) is that it can very easily be incorporated in an existing variational assimilation framework (3D-Var or 4D-Var). This is the reason, why it was selected for the HIRLAM variational data assimilation. This hybrid assimilation method has also been applied to the WRF (Weather Research and Forecasting) regional model (Wang et al., 2008a, b; Zhang and Zhang, 2012) and operationally also in the global UK Meteorological Office forecasting system (Clayton et al., 2013).

3 The HIRLAM variational data assimilation

The HIRLAM variational data assimilation includes a 3-D version (3D-Var, see Gustafsson et al., 2001 and Lindskog et al., 2001) and a 4-D version (4D-Var, see Gustafsson et al., 2012). We have incorporated the hybrid variational ensemble technique in both 3D-Var and 4D-Var.

The core elements of the HIRLAM variational data assimilation are the incremental formulation (Courtier et al., 1994), the spectral representation of the assimilation increment with a 2-D discrete Fourier series (Berre, 2000) and the

tangent-linear (TL) and adjoint (AD) models, based on the spectral version of HIRLAM, applied in 4D-Var (Gustafsson and Huang, 1996). The application of periodic functions like the discrete Fourier series over a regional model domain is made possible through an extension of the model domain in both horizontal directions to obtain bi-periodicity (Haugen and Machenhauer, 1993). Since the same discrete Fourier series and the same area extension are used to represent horizontal correlations during the data assimilation, the area extension needs to be wide enough to let these horizontal correlations fall off to zero over the width of the extension zone.

The following cost function is minimised with respect to the assimilation increment $\delta \boldsymbol{x}_{\mathrm{var}}$ in HIRLAM 4D-Var:

$$J = J_{\mathrm{var}} + J_{\mathrm{o}} = \frac{1}{2} (\delta \boldsymbol{x}_{\mathrm{var}})^T \, \mathbf{B}_{\mathrm{var}}^{-1} \delta \boldsymbol{x}_{\mathrm{var}} + \frac{1}{2} \sum_{t_k = t_0}^{t_N} (\mathbf{H}_k \mathbf{M}_k \, \delta \boldsymbol{x}_{\mathrm{var}} - \boldsymbol{d}_k)^T \, \mathbf{R}_k^{-1} (\mathbf{H}_k \mathbf{M}_k \, \delta \boldsymbol{x}_{\mathrm{var}} - \boldsymbol{d}_k) \quad (9)$$

where $\mathbf{B}_{\mathrm{var}}$ is the background error covariance, $t_k = t_0, \ldots, t_N$ the data assimilation time window, $\boldsymbol{d}_k = \boldsymbol{y}_k - H_k(M_k(\boldsymbol{x}_{\mathrm{b}}))$ the innovations with $\boldsymbol{y}_k$ being the vector of observations at time t_k, $\boldsymbol{x}_{\mathrm{b}}$ the model background state valid at time t_0, $M_k(.)$ denotes integration of the nonlinear model from time t_0 until time t_k and $\mathbf{M}_k$ the corresponding tangent linear model integration. $H_k(.)$ is the nonlinear observation operator, $\mathbf{R}_k$ is the observation error covariance and $\mathbf{H}_k$ the linearised observation operator, all valid at time t_k. The main difference between 4D-Var and 3D-Var is that for 3D-Var the assimilation increment is assumed constant in time ($\mathbf{M}_k = \mathbf{I}$) and valid in the middle of the assimilation window. For 4D-Var a weak digital filter constraint (Gustafsson, 1992; Gauthier and Thépaut, 2001) is also applied to prevent spurious growth of fast oscillations and there is also the possibility to apply relinearisations of M_k and H_k in an outer minimisation loop.

For the minimisation of the cost function J, a preconditioning transform is applied to the assimilation control variable $\chi = \mathbf{U}^{-1} \delta \boldsymbol{x}_{\mathrm{var}}$ such that the error covariance matrix for the transformed variable χ can be assumed to be diagonal. The variable transform is based on simplifying assumptions such as homogeneity and isotropy with respect to horizontal correlations. This variable transform in the HIRLAM variational data assimilation essentially follows Berre (2000) and it also includes balance operators derived by statistical regression techniques. The data assimilation control variables are vorticity, un-balanced divergence, un-balanced temperature, un-balanced surface pressure and un-balanced specific humidity, all represented by their spectral components. As an extension to the original formulation by Berre (2000), a variable Coriolis parameter is applied in the balancing between the mass field and the wind field.

4 Implementation of an ensemble constraint in the HIRLAM variational data assimilation

In the first version of the HIRLAM Hybrid variational ensemble data assimilation, we have assumed that the weights α_k, $k = 1, \ldots, K$ given to the background perturbations of the K ensemble members are functions of horizontal position only. Furthermore, since these weights now are included in the assimilation control vector, we need to specify a covariance matrix $\mathbf{A}$ to represent the characteristics of these ensemble weights. We have chosen to apply the same simplifying assumptions and pre-conditioning as in the variational minimisation, we thus assume that the horizontal correlations for the ensemble weights are homogeneous and isotropic. In addition, we specify a variance for the ensemble weights. These assumptions mean implicitly that the localisation for the covariance matrix $\mathbf{B}_{\mathrm{ens}}$ is isotropic, equivalent to what is applied with the Schur product in the localisation of background error covariances for Ensemble Kalman filters.

We apply the same ensemble weighting functions α_k, $k = 1, K$ to all model variables at all vertical levels. One needs to be a bit careful not to destroy completely the dynamical balances between the different model variables, fulfilled in the model states of each ensemble member (Kepert, 2009). We have therefore chosen to apply the weighting functions to the variables vorticity, divergence, temperature, specific humidity and ln(ps). This should give gradient relationships like geostrophic balance a better chance to survive this implicit localisation in comparison with application of the weights directly to wind components, for example.

For the ensemble constraint J_{ens} we need to specify the general weight β_{var} of the climatological background error constraint, the corresponding weight $\beta_{\mathrm{ens}} = \frac{\beta_{\mathrm{var}}}{\beta_{\mathrm{var}} - 1}$ of the ensemble constraint, the variance of the ensemble weighting function α_k, and the horizontal correlation spectrum of the ensemble weighting function α_k. These variables can be considered as tuning coefficients of the hybrid variational ensemble data assimilation. We have done experiments with full weight to the variational background error constraint, with equal weights to the two background error constraints ($\beta_{\mathrm{var}} = \beta_{\mathrm{ens}} = 2.0$) and with a strong penalty on the static background error constraint ($\beta_{\mathrm{var}} = 11.0$). In the present formulation the ensemble weighting functions are assumed to have zero mean. The standard deviation is used to control their amplitude and is set to be $\frac{1}{K}$ for each of α_k, $k = 1, \ldots, K$, where K is the ensemble size. The assumed horizontal autocorrelation function of the weights α_k expresses requirements on their smoothness. One may argue that these weights should have a sufficiently large scale to prevent important forecast errors related to, for example, baroclinic instability from being destroyed by the localisation effects. The size of the ensemble may also be a factor in choosing the localisation scale. With a smaller ensemble, the sampling error is greater and therefore a shorter localisation scale might be justified. For the first reason, however, we use the climatological

horizontal spectrum for the un-balanced surface pressure, which has the largest horizontal scales among the control variables. The shape of such a horizontal correlation function is very close to a Gaussian one. In addition, we have made experiments with other analytically specified horizontal correlation functions, similar to those that are applied for localising covariances in Ensemble Kalman filters (Gaspari and Cohn, 1999).

The *power law*

$$\rho_{\mathrm{p}}(r;\, c) = \frac{1}{1 + \frac{1}{2}\left(\frac{r}{c}\right)^2} \tag{10}$$

with r being the distance and c a parameter (the length scale), is known to have most of the energy in the long waves. This horizontal correlation function decreases with distance very slowly and is different from zero even at distances longer than 10 length scales.

The *5-th order piecewise rational function* (Gaspari and Cohn, 1999)

$$\rho_{\mathrm{c}}(z;\, c) = \begin{cases} -\frac{1}{4}\left(\frac{|z|}{c}\right)^5 + \frac{1}{2}\left(\frac{z}{c}\right)^4 + \frac{5}{8}\left(\frac{|z|}{c}\right)^3 \\ -\frac{5}{3}\left(\frac{z}{c}\right)^2 + 1, & 0 \le |z| \le c, \\ \frac{1}{12}\left(\frac{|z|}{c}\right)^5 - \frac{1}{2}\left(\frac{z}{c}\right)^4 + \frac{5}{8}\left(\frac{|z|}{c}\right)^3 \\ +\frac{5}{3}\left(\frac{z}{c}\right)^2 - 5\frac{|z|}{c} + 4 - \frac{2}{3}, & c \le |z| \le 2c, \\ 0, & |z| > 2c \end{cases} \tag{11}$$

has a very similar behaviour as the Gaussian correlation function if the scaling parameters are matched properly, but it vanishes exactly for distances larger than $2\,c$.

The *windowed power law*

$$\rho_{\mathrm{pc}}(r;\, L) = \rho_{\mathrm{c}}\left(r;\, L\sqrt{10/3}\right)\, \rho_{\mathrm{p}}(r;\, L) \tag{12}$$

is used to model correlation functions that have a relatively large amount of spectral energy on shorter waves.

Because the variational cost function is minimised in spectral space, the covariance matrix **A** includes the spectral density of the selected correlation function obtained via a 2D-Fourier transform. Since the correlation model is assumed to be homogeneous, the covariance matrix **A** is diagonal and its inverse is easily available. By definition any homogeneous correlation function has a non-negative spectrum everywhere.

The correlation functions described and discussed above are illustrated in Fig. 1.

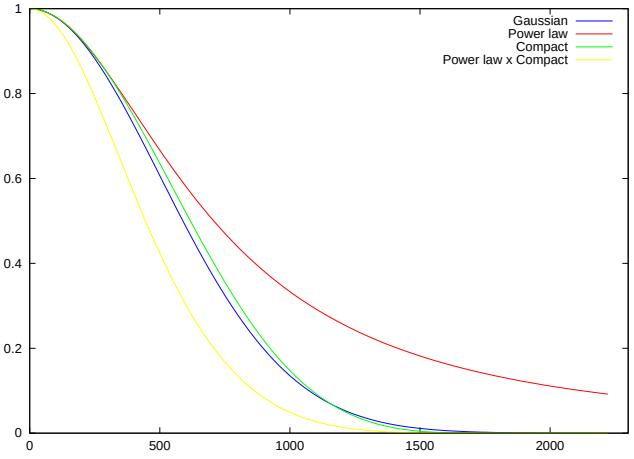

Fig. 1. The horizontal correlation functions: Power Law (red), Gaussian (blue), the Compact 5th-order piecewise rational function (green) and the windowed power law (yellow); the length scale $L = 500$ km.

5 Ensemble perturbation techniques

5.1 The ETKF re-scaling

To approximate the sequential update and the dynamical evolution of the model state covariance, we employ the hypothesis that a limited size ensemble of model states can be used to efficiently sample the leading directions of the forecast error variability. We have implemented the ETKF rescaling scheme (Bishop et al., 2001; Wang et al., 2004), a version of the Ensemble Square Root Kalman filter (Tippett et al., 2003). Under this approach, the evolution and the update of the covariance is carried out on its square-root, approximated by the ensemble of model states. The ETKF rescaling scheme uses a transform to construct the analysis square-root $(\mathbf{B}_i^{\mathrm{a}})^{1/2}$ at time t_i from the forecast square-root $(\mathbf{B}_i^{\mathrm{f}})^{1/2}$ and the non-linear dynamical model is used to propagate the error covariance in time to the next assimilation cycle.

Because the forward numerical integration of each ensemble member is the main computational burden of the scheme, we have selected a small size of the ensemble for the first implementation ($K = 12$ for a summer case and $K = 20$ for a winter case, see below). In this case, the forecast error covariance will certainly lack contributions from several important directions. Both multiplicative and additive inflations are employed to parameterize the effect of this modelling deficiency (Wang et al., 2009).

The analysis ensemble of perturbations is constructed as an additive combination of two ensembles

$$\mathbf{Z}^{\mathrm{a}} = \mathbf{Z}^{\mathrm{a},*} + \mathbf{Y}^{\mathrm{a}}, \tag{13}$$

where $\mathbf{Z}^{\mathrm{a},*}$ is the contribution from the ensemble of forecast states and $\mathbf{Y}^{\mathrm{a}}$ is the contribution from random structures of the full-rank static forecast error covariance matrix $\mathbf{B}_{\mathrm{var}}$. We have omitted the subscript i in order to simplify notations. The forecast uncertainty, represented in the ensemble, is downscaled to the analysis uncertainty using the Kalman filter theory:

$$\mathbf{Z}^{\mathrm{a},*} = \mathbf{Z}^{\mathrm{f}}\,\mathbf{C}\,\Pi\,(\mathbf{I} + \mathbf{G})^{-1/2}\,\mathbf{A}_{\mathrm{Dsc}}\,\mathbf{C}^T. \tag{14}$$

Here $\mathbf{Z}^{\mathrm{f}}$ is a matrix with the K ensemble forecast background perturbations as columns; $\mathbf{G}$ is a $(K-1)\times(K-1)$ diagonal matrix with the non-zero eigenvalues of $(\mathbf{B}^{\mathrm{f}}_{\mathrm{ens}})' = (H\,\mathbf{Z}^{\mathrm{f}})^T\,\mathbf{R}^{-1}(H\mathbf{Z}^{\mathrm{f}})$, the forecast error covariance in the observation space, normalised with the observation variance and compressed to the ensemble space; $\mathbf{C}$ is a $K\times(K-1)$ matrix containing the corresponding eigenvectors of $(\mathbf{B}^{\mathrm{f}}_{\mathrm{ens}})'$ as its columns; Π is a single coefficient and it corresponds to an adaptively estimated multiplicative scalar inflation factor, which parameterizes the effect of several aspects, such as the impact of the space compression, the effect of model errors and the impact from un-sampled directions of the leading directions of the forecast error uncertainty; Π is typically around 15 with 20 ensemble members in the present setup; $\mathbf{A}_{\mathrm{Dsc}}$ is an empirical diagonal downscaling matrix, which prohibits the amplification of uncertainty in the non-leading directions (Bojarova et al., 2011).

The forecast perturbations are rotated along the eigenvectors of $(\mathbf{B}^{\mathrm{f}}_{\mathrm{ens}})'$, the rotated perturbations are downscaled with the weights proportional to the eigenvalues of the $(\mathbf{B}^{\mathrm{f}}_{\mathrm{ens}})'$ and are rotated backwards. The backwards rotation assures the centering of the rotated perturbations around the mean optimally using the available degrees of freedom (Wang et al., 2004). Both the geometry and the precision of the observational network are taken into account for transforming the forecast perturbations into the analysis perturbations. Only conventional observations (TEMP, PILOT, SHIP, AIREP, DRIBU, SYNOP) were used for constructing the rescaling in a summer test case, while satellite radiance data (AMSU-A) were used in addition for a winter test case. For 4D-Var, the forecast ensemble perturbation input to the estimation of the forecast error covariance in observation space is provided at the observation time windows (with a time resolution of 1h), while for 3D-Var the corresponding forecast ensemble perturbation input is given for the nominal analysis time only.

The impact from the random structures of the climatological covariance matrix, an additive inflation of the analysis error variance, supply the ensemble with a "fresh blood" each assimilation cycle and helps to recover important uncertainties not included in the small ensemble originally.

The ensemble re-scaling scheme is adopted for application to a Limited Area Model. The ETKF perturbations are relaxed towards the EuroTEPS perturbations (Frogner and Iversen, 2002) on the lateral boundaries and in the stratosphere (above 100 hPa).

The ETKF rescaling scheme iteratively estimates the leading directions of the forecast error variability. By sequentially applying this scheme an ensemble of perturbations, which contains flow dependent structures and reflects both the density and the quality of the observational network, can be created. However, the severe rank deficiency of the forecast and analysis error covariances under affordable sizes of the ensemble is a weak point of the ETKF rescaling scheme. The multiplicative variance inflation is introduced to make these rank-deficient covariances physically meaningful, and is a core issue for the efficient performance of the ETKF rescaling scheme. The variance inflation is calculated iteratively by adjusting the ensemble spread to the innovation variance (corrected for the observation error variance), averaged over the whole observation space.

The observational error variance is tuned for the optimal performance of the variational data assimilation scheme (Dee, 1995). It provides the mechanism which controls to what extent the information from the observations of a certain type should influence the numerical model. There is a certain inconsistency between the assumption on the observational error variance $\mathbf{R}$ and the fit of $\mathbf{R}$ to the innovations. This makes the estimation of the multiplicative inflation less efficient. For more details on the ETKF re-scaling as implemented in HIRLAM, see Bojarova et al. (2011).

5.2 The Ensemble of Data Assimilations (EDA)

An alternative to the ETKF re-scaling is to run an Ensemble of Data Assimilations (EDA) with perturbation of data assimilation input data (observations and background). In case of a perfect model assumption, perturbations of the background correspond to the forecast evolution of the previous analysis perturbations. Several operational Ensemble Prediction Systems (EPSs) are based on such EDA schemes, for example the EPS systems of ECMWF and Meteo-France, which use 4D-Var in the assimilation for each ensemble member. The Canadian operational EPS system is based on an Ensemble Kalman Filter that also applies perturbation of observations.

We will apply the 3D-Var hybrid, as described above, without perturbation of observations for the ensemble control and with perturbation of observations for the other ensemble members. The observation perturbations are generated as Gaussian random numbers $N(0, \sigma_{\mathrm{obs}})$ which are added to all types of observed values that enter into the data assimilation, with σ_{obs} being the same observation error standard deviation that is applied in the variational data assimilation (the $\mathbf{R}$-matrix). This approach to observation perturbation may possibly not be the most optimal one, since some of the σ_{obs}-values have been assigned to provide a proper influence of each type of observation and not only to represent the observation error including representivity errors. Negative average effects of the crudely designed observation perturbation scheme is, however, partly compensated by a final tuning of the analysis perturbations through a multiplicative inflation factor, estimated in the same way as for the ETKF re-scaling scheme i.e. through a comparison between the background forecast perturbation variance and the innovation variance corrected for the observation error variance. This multiplicative inflation also acts to take account of model errors.

Table 1. Description of experiments carried out with the HIRLAM Hybrid variational ensemble data assimilation for the period 12–24 August 2007.

Experiment name	Description
3DVAR	3D-Var, no ensemble constraint
hybrid_90	3D-Var Hybrid, $\beta_{\mathrm{var}} = 11$ (90 % ensemble, 10 % static cov.) Ensemble weight spectrum as for p_{s} Tuning factor $\kappa = 1.0$
hybrid_50	3D-Var Hybrid, $\beta_{\mathrm{var}} = 2$ (50 % ensemble, 50 % static cov.) Ensemble weight spectrum as for p_{s} Tuning factor $\kappa = 1.0$
hybrid_pwl_500	3D-Var Hybrid, $\beta_{\mathrm{var}} = 2$ (50 % ensemble, 50 % static cov.) Ensemble weight spectrum by a power law with length scale 500 km Tuning factor $\kappa = 1.0$
hybrid_pwl_200	3D-Var Hybrid, $\beta_{\mathrm{var}} = 2$ (50 % ensemble, 50 % static cov.) Ensemble weight spectrum by a windowed power law with length scale 200 km Tuning factor $\kappa = 1.0$

6 Data assimilation experiments

Real observation data assimilation and forecast experiments were carried out on the model domain illustrated in Fig. 2 for the short summer period 12–24 August 2007. The horizontal grid resolution was 22 km, the number of vertical levels was 40 and the number of ensemble members was 12. In order to test the impact of the hybrid assimilation, data assimilation experiments were also carried out for a longer winter period 17 January–29 February 2008 over a similar domain as illustrated in Fig. 2, also with 40 levels but with a finer horizontal grid resolution of 11 km. The number of ensemble members for these experiments was 20 and the data assimilation was carried out with a 6 h cycle.

The forecast model used in the experiments was the HIRLAM grid point forecast model. It is hydrostatic and it utilises a semi-implicit, semi-Lagrangian two time level time integration scheme (Undén et al., 2002). The physical parameterizations used were the CBR turbulence scheme (Cuxart et al., 2000), the Kain-Fritsch convection scheme (Kain, 2004), the Rasch–Kristjánsson cloud water scheme (Rasch and Kristjánsson, 1998), the Savijärvi (1990) radiation and the ISBA surface scheme (Noilhan and Mahfouf, 1996), supplemented with new formulations for the heat transfer in the soil and in a snow layer (S. Gollvik, personal communication, 2013).

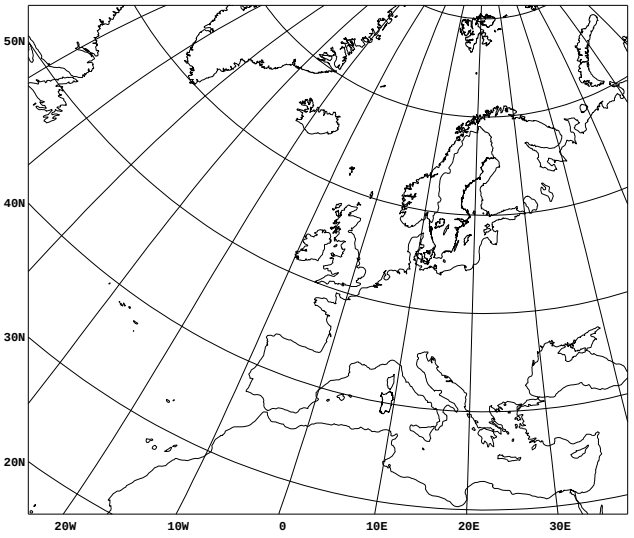

Fig. 2. Model domain for the summer case Hybrid variational ensemble data assimilation experiments.

6.1 Results from the summer period experiments

Experiments for the summer period were carried out in accordance with the descriptions in Table 1.

6.1.1 Estimated ensemble background error variances

The background error variance (σ_{b}^2) is an important quantity that together with the observation error variance (σ_{o}^2) determine the magnitude of the weight given to the observations. It is therefore of interest to investigate the flow-dependent background error variance fields provided by the ETKF based ensemble for the +6 h forecast. We will show examples of the ensemble based background error variance applied for the assimilation at 21 August 2007 12:00 UTC. The corresponding background model state, i.e. the +6 h forecast from 21 August 06:00 UTC is illustrated for 300 hPa geopotential and wind in Fig. 3 (left panel) and for 850 hPa temperature in Fig. 3 (right panel). In the upper levels we may notice a strong meridional circulation with a meandering jet-stream over the North Atlantic. Associated with this is a high pressure ridge along 20° W towards Iceland and a low pressure system (trough) centred over France. Also note a small scale cut-off low at 35° N 30° W. In the 850 hPa temperature we may notice strong gradients (fronts) associated with the cut-off low over the Atlantic and also in the area of the upper-air trough over Western Europe.

Examples of the ensemble estimate of the background error variance fields, associated with the background model state illustrated in Fig. 3, are presented in Fig. 4. We have chosen to show the variance fields for wind components at model level 10 (approximately 300 hPa, left panel) and temperature at model level 30 (approximately 850 hPa, right panel). The corresponding climatological background error

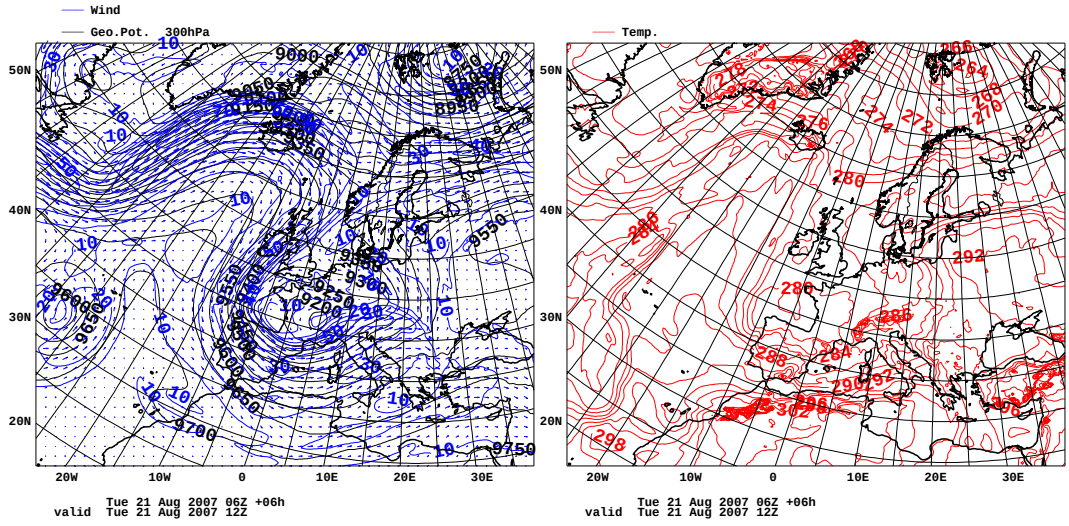

Fig. 3. 300 hPa wind and geopotential height (left panel) and 850 hPa temperature (right panel) taken from the background model state at 21 August 2007 06:00 UTC + 6 h; experiment based on equal static and ensemble contributions to the background error variance. Isoline spacing 50 m, 10 m s^{-1} and 2 K.

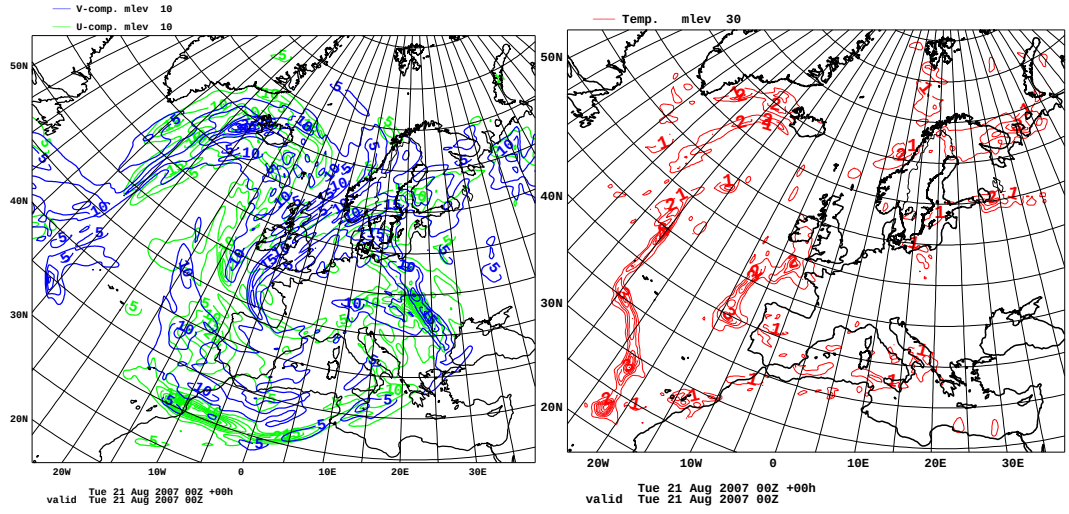

Fig. 4. Examples of estimated background error variance fields based on the ensemble of +6 h forecast valid at 21 August 2007 12:00 UTC from the hybrid data assimilation experiment hybrid_50. Wind components at model level 10 (approximately 300 hPa, left panel) and temperature at model level 30 (approximately 850 hPa, right panel). Isoline spacing 5 m^2 s^{-2} and 1 K^2.

variance fields are constant in the horizontal for the wind components and have a dependence on latitude for the temperature, due to the use of a variable Coriolis parameter in the balancing between vorticity and linearised geopotential. The first to be noticed in Fig. 4 is the strong inhomogeneity of the variance fields contrasting radically the assumptions on homogeneity in 3D-Var. Furthermore, areas of large background error variance are clearly related to features in the background model state, providing support to the core idea of this study, to introduce flow-dependent background error statistics into the data assimilation process. To mention a few details, large uncertainties seem to be associated with the position and the strength of the meandering jet-stream over the North Atlantic. The association of large background error variances with the jet-stream is easily understandable. The horizontal wind shear close to the jet stream is large and even small errors in the forecast horizontal position of the jet-stream will give rise to large absolute errors, measured in m s^{-1}. Furthermore, the jet stream is often associated with a large vertical wind shear and dynamical instability. To handle this dynamical source of uncertainty in upper-air data assimilation, one does not necessarily need to introduce the utilisation of ensembles, it was shown by Lindskog et al. (2006)

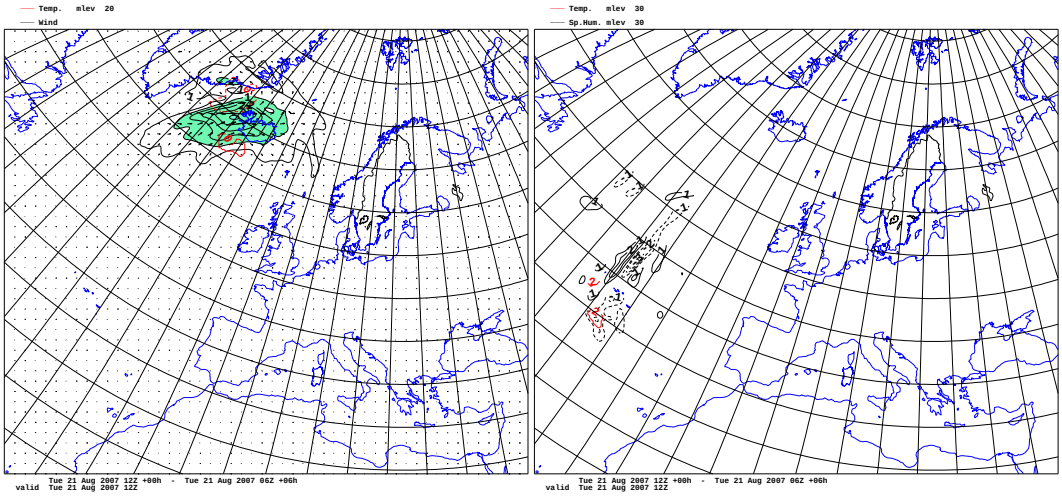

Fig. 5. Assimilation increments from single simulated observation experiments. Left panel: wind and temperature increments at 300 hPa (a westerly wind observation increment of 5 m s^{-1} was inserted on 300 hPa at 65° N 25° W), isoline spacing 1 m s^{-1} and 1 K; right panel: temperature and specific humidity increments at 850 hPa (temperature observation increment of 5 K was inserted on 850 hPa at 40° N 30° W), isoline spacing 0.1 K and 0.0001.

that a diagnostic interpretation of instability can be applied successfully.

Concerning the horizontal variability of the background error variance fields for low level temperature (Fig. 4, right panel), we can notice that large values occur in very elongated (anisotropic) structures. Comparing with the background model state for 850 hPa temperature in Fig. 3 (right panel), it is clear that these large background error variances are associated with the occurrence of atmospheric fronts. One may in particular notice the frontal systems in the vicinity of the upper-air cutoff low at 35° N 30° W.

We can say that the dynamical propagation of an ensemble of model states, together with the ETKF re-scaling to estimate an ensemble of analysis perturbations, have provided us with a robust tool to describe the background error uncertainty as influenced by dynamical as well as observation network effects.

6.1.2 Single observation impact experiments

We illustrate here the possibilities of the Hybrid Variational Data assimilation to resolve flow-dependent structures through a "single simulated observation" experiment. A single simulated observation is inserted into the data assimilation process. The impact on the model state from such an observation in a totally controlled environment can tell about what cross-correlations between model state components are implied by the variational or hybrid covariance models. In Fig. 5 we show the data assimilation increments from two "single observation" experiments with the version of the hybrid ETKF-Variational data assimilation assuming 90 % contribution to the background covariance from the ensemble component (experiment hybrid_90). A simulated wind observation at 300 hPa was inserted in the jet-stream to the west of Iceland, and a temperature observation was inserted at 850 hPa within the front associated with the upper-air low-pressure cut-off at 35° N 30° W. These experiments demonstrate the advantages of the hybrid data assimilation system in resolving flow-dependent structures (results from reference single observation experiments based on climatological background error covariances are not shown here, but could be found elsewhere; Gustafsson et al., 2001). At the same time they reveal weaknesses of this first implementation of a hybrid assimilation. We seem to be able to modify and move an atmospheric front in a consistent manner ("an old dream of an old data assimilation worker") with the hybrid data assimilation. On the other hand, the analysis increments, especially of temperature and humidity (not shown), are too noisy and the wind increments in the jet stream are overestimated. The ensemble size of only 12 members, used in these experiments due to technical reasons, must be increased. A decrease of the decorrelation scale of the correlation functions $\rho(r)$, which imposes the smoothness requirements on the local perturbation weights, can be used to remove the noise to a certain extent. However, in this case, informative structures of the ensemble associated with the large scale motion are lost as well. We consider that an increase of the ensemble size is the only way to tackle the rank-deficiency problem and, thus, the spurious correlations at large distances.

Furthermore, the ensemble spread of the temperature is too small and the ensemble spread of wind is too large. The analysis increments are of order tenths of a degree, although the inserted innovation was 5° large. One reason is certainly the rank-deficiency of the ETKF ensemble, which requires the application of a multiplicative inflation. The multiplicative inflation is estimated in a too simplistic manner. Another

reason lies in the assumptions on the observation error variances. The observation error for temperature measurements is assumed to be relatively small in the HIRLAM data assimilation system. As a result, following the variance update equation, the variance of the analysis error for temperature and therefore the spread of the ensemble for temperature becomes too small. A re-tuning of the observation error variances is required for the optimal performance of the hybrid data assimilation system.

6.1.3 Comparison of real observation assimilation increments

The final outcome of the whole data assimilation process are the data assimilation increments. We will illustrate here the data assimilation increments for 21 August 2007 12:00 UTC, thus for the same moment of time for which we have described and discussed the background error variances and the simulated single observation experiments above. The comparison between the different assimilation increments is not completely clean, since the background states and thus the observation innovations differ. We will concentrate our comparison on the effects of the different applied spectral densities for the ensemble perturbation weights. All experimental results to be described are from experiments with a 50 % contribution from the climatological component and with a 50 % contribution from the ensemble component to the background error covariance.

Assimilation increments for wind components at model level 10 and for temperature at model level 20 are presented in Fig. 6 for four different experiments: for the 3D-Var experiment (experiment 3DVAR, upper left panel) and for the hybrid experiments with three different spectral density formulations for the ensemble perturbation weights, the spectral density used for un-balanced surface pressure in 3D-Var (experiment hybrid_50, upper right panel), the power law spectral density with a length scale of 500 km (experiment hybrid_pwl_500, lower left panel) and for the windowed power law spectral density with a length scale of 200 km (experiment hybrid_pwl_200, lower right panel).

The first to notice for the assimilation increments in Fig. 6 are the smooth, large scale and almost circular increments from the 3D-Var experiment (upper left map) and the occurrence of more elongated (anisotropic) increment structures in the first hybrid experiment (upper right map). We can clearly see similarities to the flow structures in the background field (Fig. 3). Secondly, we may notice that the flow-dependent elongated structures are further enhanced when a larger scale localisation is applied for the ensemble perturbation weights (lower left map). Finally, by introducing a rather small scale localisation, through the windowed power law with a length scale of 200 km, we see that these flow-dependent elongated flow increment structures almost disappear. The increment map from this experiment appears much like the 3D-Var increment map (compare the lower right map in Fig. 6 with the upper left map).

From this comparison of real observation increments we may conclude that it is crucially important to pay attention to details in the formulation of the spatial characteristics of the localisation of the ensemble perturbation weights. A too small scale localisation may introduce smoothing effects in the extended ensemble space that can completely wipe out all the potential benefit from taking an ensemble of model background states into account.

6.1.4 Verification of forecasts based on real observation assimilation experiments

Forecasts up to +48 h were carried out at 00:00 and 12:00 UTC for all the five experiments described in Table 1. We have verified these forecasts against all available radiosonde and surface (SYNOP) observations within the model domain. The data assimilation experiments were carried out for the period 12–24 August 2007. We restricted the verification to the period 16–24 August 2007, thus allowing an ensemble perturbation spin up during 4 days.

A period of 8 days is certainly far too short to make any definite conclusions about the performance of the hybrid variational ensemble data assimilation, the data period was selected for practical reasons, since we had available a first HIRLAM ensemble prediction setup for this period including ensemble based lateral boundary conditions from EuroTEPS experiments.

First we investigate the effects of varying the weight (β_{var}) given to the climatological background error constraint and the weight given to the ensemble background error constraint (β_{ens}). For this purpose, bias and RMS (Root Mean Square) verification scores for temperature, wind speed and relative humidity forecast profiles as verified against radiosonde observations averaged over the period 16–22 August 2007 and over +12, +24, +36 and +48 h forecasts are shown in Fig. 7. The results from experiments 3DVAR (3D-Var), hybrid_90 (10 % 3D-Var and 90 % ensemble covariance), and hybrid_50 (50 % 3D-Var and 50 % ensemble covariance) are compared.

The verification scores in Fig. 7 provide quite a consistent result. We may notice that the forecasts from the 3D-Var experiment have better scores for temperature and wind while the scores for humidity are slightly worse in the upper troposphere (above 700 hPa) compared to those for the experiment with the ensemble dominant background covariance. The most important result in Fig. 7 is that the experiment based on equal weights ($\beta_{\mathrm{var}} = \beta_{\mathrm{ens}}$) given to the climatological and the ensemble based parts of the background error covariance provides the best forecast verification scores for all the three basic model variables at all vertical levels. This is a very encouraging result that gave us confidence to continue the developments along the ideas of a hybrid variational ensemble data assimilation.

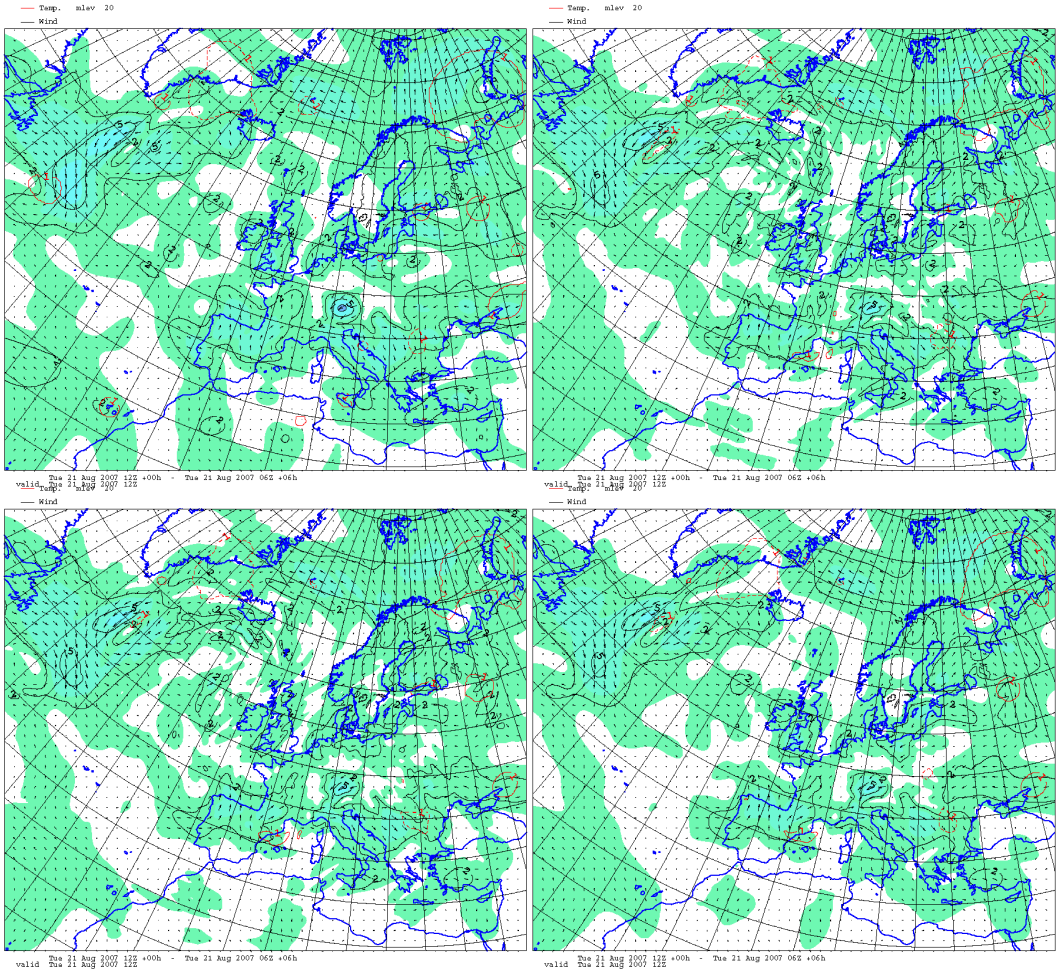

Fig. 6. Example of assimilation increments for wind speed at model level 10 (black lines and colour-shading) and temperature at model level 20 (red lines) on 21 August 2007 12:00 UTC. 3D-Var (upper left panel); hybrid with different horizontal spectral densities for the ensemble weights: same spectral densities as for assimilation of un-balanced surface pressure in 3D-Var (upper right panel), spectral density corresponding to a power law correlation with 500 km length scale (lower left panel) and spectral density corresponding to a windowed power law correlation with a 200 km length scale (lower right panel). All experiment are based on a 50 % contribution from the climatological component and a 50 % contribution from the ensemble component to the background error covariance. Isoline spacing 2.5 m s^{-1} and 1 K. Different shades of green indicate the intervals between 1, 3, 6, 8 and 10 m s^{-1}.

In order to shed some more light on how the formulation influences the background error covariance, we have selected one of the model variables, the temperature at 700 hPa, and illustrated the time-averaged forecast scores as a function of forecast length in Fig. 8. Here it is interesting to note that the 3D-Var assimilation gives the closest fit to the observations at analysis time with a RMS difference of approximately 0.5 K, while the corresponding RMS difference for the assimilation based on a 90 % contribution from the ensemble based covariance (experiment hybrid_90) is approximately 0.9 K and thus almost doubled. The corresponding RMS fit for the assimilation scheme based on equal weights to the climatological and the ensemble parts of the background error covariance (experiment hybrid_50) is approximately 0.6 K and lies thus in between the RMS of the other two experiments, as can be expected. The analysis model state fits closer to the observations in the 3D-Var experiment in comparison with the two experiments, when also the ensemble based background error covariance was partly utilised. This is consistent with the magnitudes of the corresponding background error variance fields of the two components, as discussed and illustrated above. The climatological background error variance has quite a large value and is more or less constant over the whole model domain ("we do not know where we can expect large background errors"), while the ensemble based variance has a large amplitude in quite restricted areas ("the model dynamics and the history of spatial observation distributions provides some information on background error uncertainty"). It needs to be mentioned that the low rank of the ensemble covariance may also contribute to the poorer

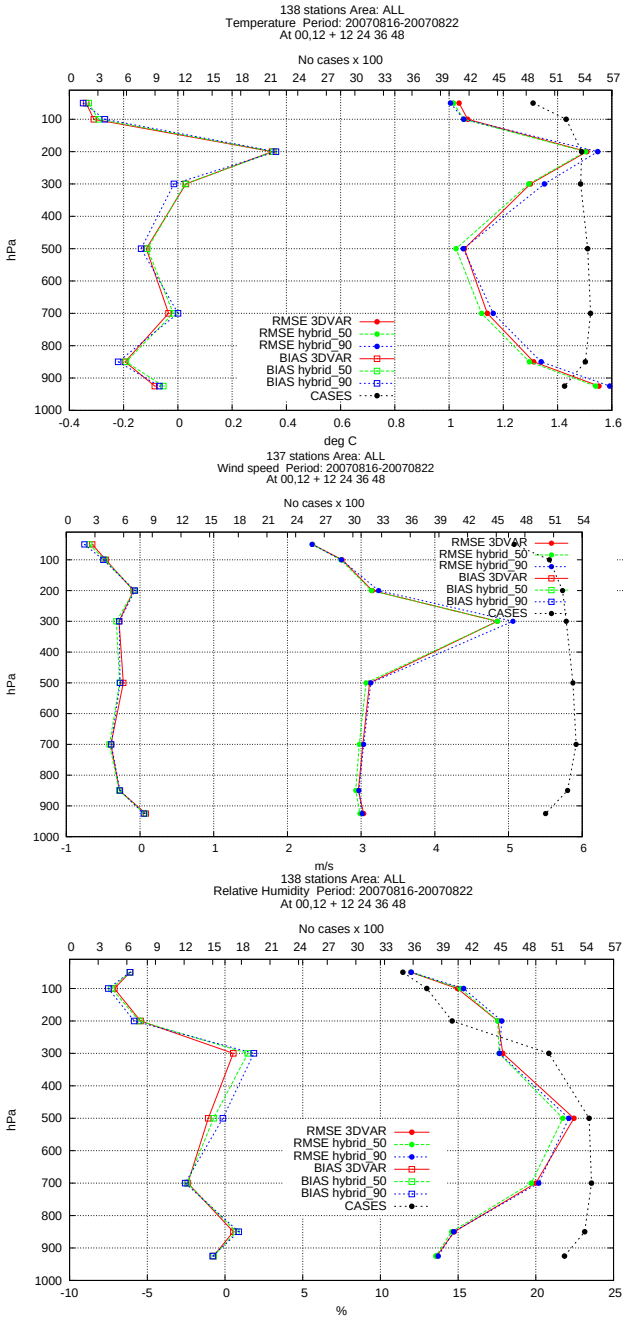

Fig. 7. Bias and RMS (Root Mean Square) verification scores for temperature (upper panel), wind speed (middle panel) and relative humidity (bottom panel) forecast profiles as verified against radiosonde observations averaged over the period 16–22 August 2007 and over +12, +24, +36 and +48 h forecasts. Experiments 3DVAR (3D-Var, red curves), hybrid_90 (10 % 3D-Var and 90 % ensemble covariance, blue curves) and hybrid_50 (50 % 3D-Var and 50 % ensemble covariance, green curves). The curve marked CASES indicates the number of observed values for the verification.

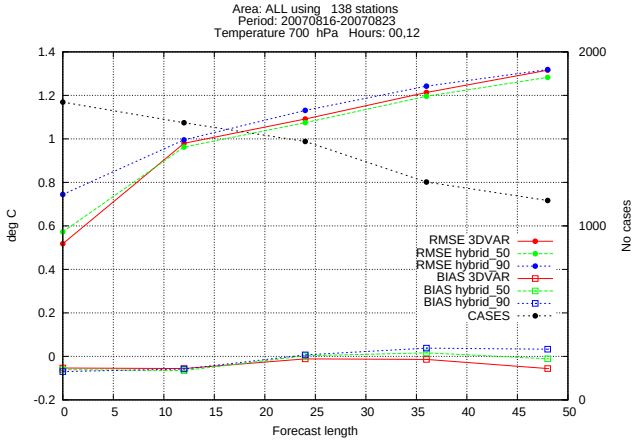

Fig. 8. Bias and RMS (Root Mean Square) verification scores for 700 hPa temperature forecasts as verified against radiosonde observations averaged over the period 16–22 August 2007 as a function of forecast length. Experiments 3DVAR (3D-Var, red curves), hybrid_90 (10 % 3D-Var and 90 % ensemble covariance, blue curves) and hybrid_50 (50 % 3D-Var and 50 % ensemble covariance, green curves). The curve marked CASES indicates the number of observed values for the verification.

fit to the observations in the case of the hybrid analysis, as compared to 3D-Var, in particular where the observations are dense (Clayton et al., 2013).

Although the fit to the observations is closest for the 3D-Var assimilation scheme in Fig. 8 at analysis time, we can notice that already at a forecast length of +12 h this is no longer the case. The fit to observations is now closest for the experiment based on equal weights to the climatological and the ensemble part of the background error covariance. This tendency for the experiment with equal contributions to the background error covariance to have smaller RMS forecast verification scores becomes more pronounced with forecast length.

We have presented and discussed forecast verification scores as a function of forecast length for 700 hPa temperature only. The patterns for the development of the forecast scores for other model variables (figures are not shown) are very similar to the pattern for the 700 hPa temperature. We have also investigated the effects of varying the horizontal spectral density for the weights given to the different ensemble members in the assimilation increment, i.e. the definition of the covariance matrix **A** in the ensemble part of the background error constraint. The sensitivity of the forecast verification scores to the spectral density used, which constrains the weights given to the different ensemble members, is quite small in general (not shown here). One may possibly conclude that there is some small preference to apply the power law spectral density with a length scale of 500 km with regard to the quality of humidity forecasts.

6.2 Results from the winter period experiments

Experiments for the winter period 17 January–29 February 2008 are briefly described in Table 2. For all experiments, a 6 h data assimilation cycle was applied. For the 4D-Var experiments a 6 h assimilation window centred around the nominal analysis time was applied, while in the 3D-Var experiments a similar assimilation window was applied with the background field for calculation of innovations evaluated at the time of the observations (FGAT = First Guess at Appropriate Time). Tuning factors β_{var} and κ were set differently for 3D-Var Hybrid and 4D-Var Hybrid, and were based on separate tuning experiments to optimise the forecast performance.

Lateral boundary conditions for all experiments were provided by the global EuroTEPS low resolution forecasts, since it was required to have ensemble perturbations also on the lateral boundaries. One control experiment was repeated with high resolution deterministic ECMWF forecasts for the lateral boundary conditions, in order to investigate possible negative effects of the low resolution EuroTEPS lateral boundary conditions. Indeed, this experiment (results are not shown) indicated such negative effects of the low resolution EuroTEPS lateral boundary conditions.

The winter period experiments were run with 20 ensemble members. Generally speaking, EnKF applications for full-scale NWP models have been reported to need ≈ 100 ensemble members for a good performance. Such a large number of ensemble members was out of reach for our investigation. One of our 4D-Var hybrid experiments applied a double number (= 40) of ensemble members during the hybrid assimilation by adding also ensemble member forecasts valid 2 h into the data assimilation window. The idea behind selecting such a lagged valid time ensemble was the possibility to correct timing errors (and implicitly spatial phase errors) in the background field during the assimilation.

Table 2. Description of experiments carried out with the HIRLAM Hybrid variational ensemble data assimilation for the winter period 17 January–29 February 2008.

Experiment name	Description
3dvar_ref1	3D-Var, no ensemble constraint.
3Dvar_hybrid1	3D-Var Hybrid, $\beta_{\mathrm{var}} = 2$ (50 % ensemble, 50 % static cov.), Tuning factor $\kappa = 2.0$
4dvar_ref1	4D-Var, no ensemble constraint.
4dvar_hybrid1	4D-Var Hybrid, $\beta_{\mathrm{var}} = 4$ (25 % ensemble, 75 % static cov.), Tuning factor $\kappa = 4.0$
4dvar_hybrid2	4D-Var Hybrid, $\beta_{\mathrm{var}} = 4$ (25 % ensemble, 75 % static cov.), Tuning factor $\kappa = 4.0$ Ensemble perturbations for Hybrid complemented with perturbations with a +2 h lagged valid time.
EDA_hybrid1	3D-Var Hybrid, $\beta_{\mathrm{var}} = 2$ (50 % ensemble, 50 % static cov.). Generation of ensemble perturbations through an ensemble of 3D-Var assimilations with perturbed observations. Tuning factor $\kappa = 2.0$

6.2.1 Impact of the hybrid assimilation approach on top of 3D-Var and 4D-Var

For the validation of the impact of the hybrid approach on top of 3D-Var and 4D-Var we will first illustrate how the ETKF re-scaling handles the ensemble spread for temperature at model level 28 (≈ 800 hPa) in Fig. 9 (the effects of the tuning factor κ are not included). For 3D-Var hybrid (upper maps) and 4D-Var hybrid (lower maps) we present the ensemble standard deviations (ensemble spread) both before the ETKF re-scaling (maps to the left) for the background forecast fields, and after the ETKF re-scaling (maps to the right) for the analysis fields. The dynamical features of these standard deviation fields are obvious with elongated structures along atmospheric fronts, for example. Note that the standard deviation fields have a slightly smaller amplitude in the 4D-Var hybrid case than in the 3D-Var hybrid case, consistent with the generally smaller errors in short range forecasts produced from 4D-Var initial data as compared to 3D-Var based forecasts. Furthermore, note the reduction of the spread in the analysis ensemble after the ETKF re-scaling, corresponding to the effect of using observations in the assimilation process. It can also be noticed that the dynamical features are well preserved during the re-scaling process. We have shown the ensemble spread for the 4D-Var based +6 h forecast in Fig. 9 (lower left panel). It needs to be mentioned that it is the 4D-Var based +3 h forecast, valid at the start of the 4D-Var assimilation window, that enters the implicit ensemble covariance calculations in the 4D-Var hybrid assimilation, while for the 3D-Var hybrid the corresponding +6 h forecast is used. Since the spread of the +3 h ensemble forecasts generally is smaller than for the +6 h ensemble forecasts, application of different tuning factors κ for 3D-Var and 4D-Var hybrid assimilation (see Table 2) can be motivated. Note also in Table 2 that a different partitioning between the static and the ensemble background error covariances is used for 4D-Var hybrid (75 % for the static part of the covariance) as compared to 3D-Var hybrid (50 % for the static part of the covariance). The motivation for this difference is that 4D-Var partially develops its own flow-dependent background error covariances. An assimilation and forecast test over a shorter period confirmed that this choice of partitioning was a good one.

The hybrid variational ensemble data assimilation does not only utilise flow-dependent background error standard

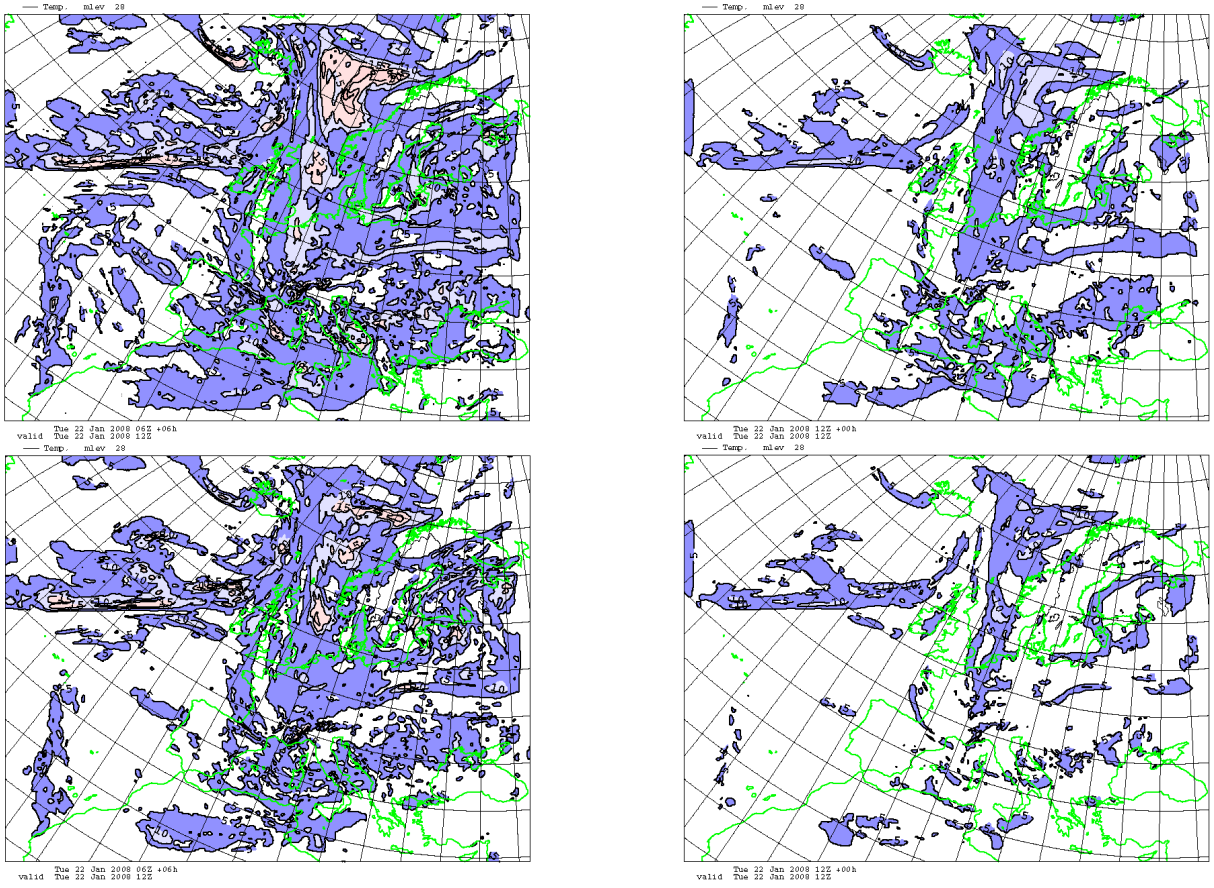

Fig. 9. Ensemble spread (RMS) for temperature at model level 28 ($\approx$ 800 hPa), 3D-Var hybrid (top panels) and 4D-Var hybrid (bottom panels), before ETKF re-scaling (left panel) and after ETKF re-scaling (right panels), 22 January 2008 12:00 UTC. Isoline spacing 0.5 K. The tuning factor κ has not been taken into account.

deviation fields as illustrated in Fig. 9. Also spatial correlations and cross-correlations between different model variables are taken into account through the ensemble information. We illustrate this here for 3D-Var and 3D-Var hybrid specific humidity assimilation increments at model level 30 ($\approx$ 850 hPa) in Fig. 10. We take specific humidity as an example because a large positive impact in humidity forecast scores was found with the hybrid 3D-Var assimilation (see below). We may notice that completely different spatially elongated structures are seen in the 3D-Var hybrid assimilation increments (Fig. 10, bottom panel) as compared with the standard 3D-Var assimilation increments (Fig. 10, top panel), for which the effects of the assumptions of isotropy and homogeneity are recognisable. With regard to the magnitudes and the sign of the increments in different areas it is not so difficult to realise that the observed innovation input to the assimilation from the sparse radiosonde network could be very similar, the main difference is that the ensemble information provides a set of flow-dependent basis functions that is used for the spatial spreading of the observed innovation information.

The impact of the hybrid assimilation for 3D-Var and 4D-Var on mean sea level pressure forecasts over a Scandinavian domain is presented in Fig. 11. Included in the figure are verification curves (bias and standard deviation) for 3D-Var, 3D-Var hybrid, 4D-Var and 4D-Var Hybrid.

From Fig. 11 it can be seen that 3D-Var hybrid provides a large positive impact on standard deviation forecast verification scores in comparison with the standard 3D-Var. The standard 4D-Var provides an even larger (doubled) positive impact over the standard 3D-Var, which is consistent with previous comparisons between HIRLAM 3D-Var and 4D-Var (Gustafsson et al., 2012). On the other hand, it is also obvious from Fig. 11 that the 4D-Var hybrid provides no positive impact over the standard 4D-Var for the mean sea level pressure standard deviation forecast verification scores during this experiment period of 40 days, a minor positive impact of the hybrid in the bias verification scores can be noticed, however.

The differences between average root-mean-square (RMS) verification scores for 3D-Var and 3D-Var hybrid are significant for +12, +18 and +24 h forecasts according to a

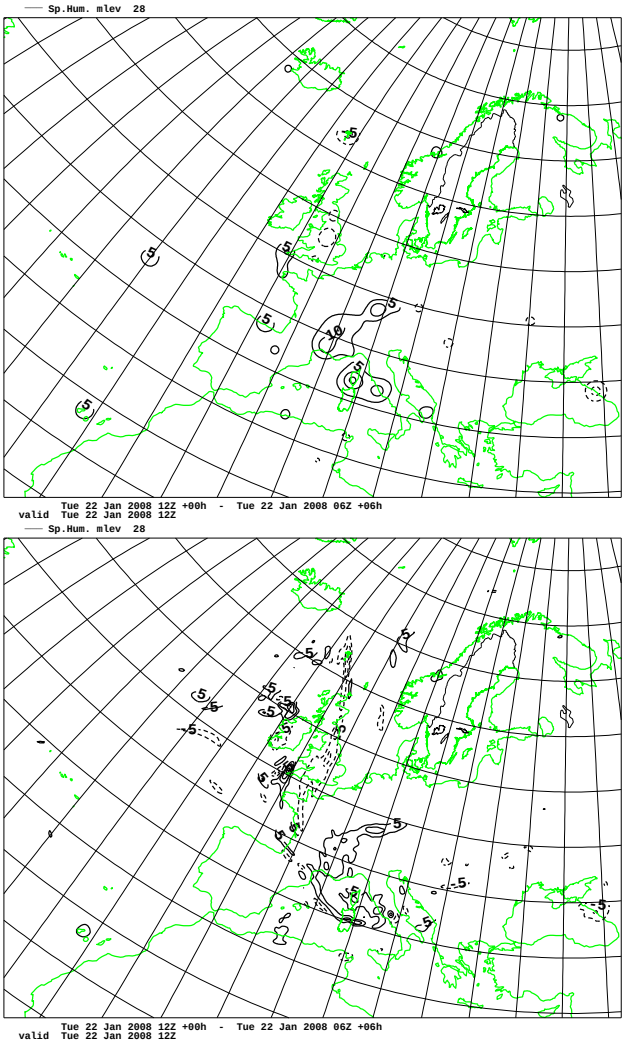

Fig. 10. Specific humidity assimilation increments at model level 30 (≈ 850 hPa) with 3D-Var (top panel) and with 3D-Var Hybrid (bottom panel). 22 January 2008 12:00 UTC. Isoline spacing 0.0005.

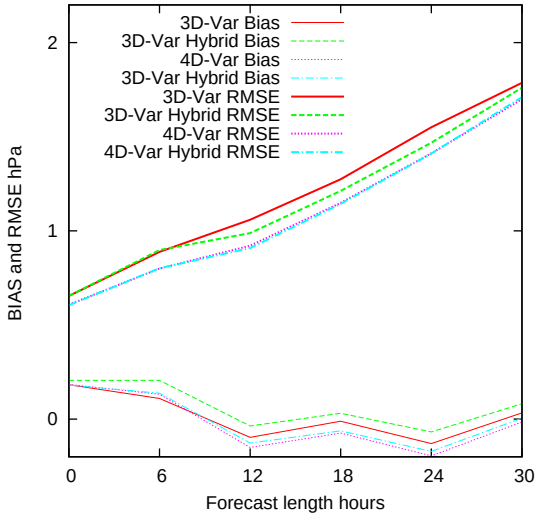

Fig. 11. Bias and standard deviation verification scores for mean sea level pressure forecasts over a Scandinavian domain averaged over the period 19 January–29 February 2008 and given as functions of forecast length. The control forecasts from the 3D-Var (red curve), the 3D-Var hybrid (green curve), the 4D-Var (blue curve) and the 4D-Var hybrid (pink curve) experiments are included. Forecasts have been run with 6th hourly lateral boundary conditions.

two-sided student *t* test, the differences between the 4D-Var and the 3D-Var RMS verification scores are significant for +6, +12, +18 and +24 h forecasts according to the same test.

The wind speed and relative humidity vertical profile forecast verification scores, as verified against all radiosonde stations within the forecast domain, for the 3D-Var, 3D-Var hybrid, 4D-Var and 4D-Var hybrid experiments are included in Fig. 12. With regard to the wind speed profile verification scores, we see a significant, positive impact of the 3D-Var hybrid as compared to the standard 3D-Var as well as a significant, positive impact of the standard 4D-Var over the standard 3D-Var, similarly to what was achieved for mean sea level pressure verification scores. In addition, we can now also observe a positive impact of the 4D-Var hybrid as compared to the standard 4D-Var. The positive impact of the hybrid approach is consistent over all vertical levels, for 3D-Var as well as for 4D-Var. The differences between RMS verification scores, for the 3D-Var versus the 3D-Var hybrid as well as for the 3D-Var versus the 4D-Var scores are significant at the 95 % significance level for all levels in the troposphere for wind speed.

For the forecast relative humidity profile verification scores, we notice a positive impact of the 3D-Var hybrid as compared to the standard 3D-Var and also for the 4D-Var hybrid as compared to the standard 4D-Var in the troposphere. The improvement of the verification scores are most significant for the 3D-Var hybrid as compared to standard 3D-Var, such that the 3D-Var hybrid verification scores are even better than the 4D-Var hybrid verification scores for levels in the lower troposphere where moisture is important for forecasting of weather parameters like precipitation. One may speculate why we have this very significant positive impact of the hybrid for 3D-Var and not for 4D-Var. One reason may be that the 3D-Var hybrid utilises directly the humidity spatial covariances and cross-covariances derived from the nonlinear model integration of the ensemble members, compare the increment maps seen in Fig. 10, while in the case of the 4D-Var these nonlinear model ensemble covariances and cross-covariances are implicitly transformed to be valid at the actual observation time by the integration of the tangent linear model. In case the tangent linear model is not very accurate for humidity, this transformation may degrade the quality of the humidity covariances and cross-covariances. This is likely to be the case for the tangent linear model in HIRLAM

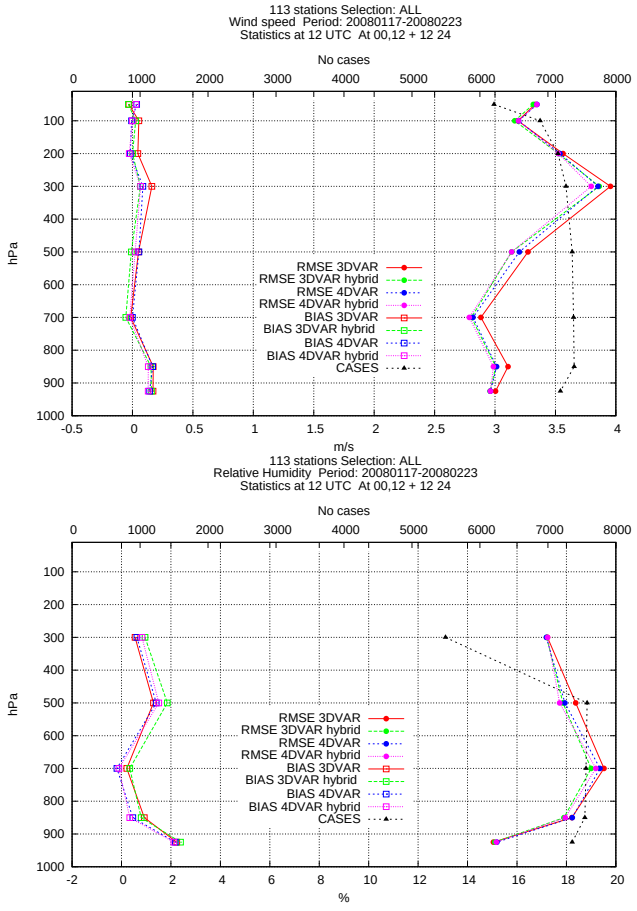

Fig. 12. Bias and standard deviation verification scores for wind speed (upper panel) and relative humidity (lower panel) profile forecasts as verified against radiosonde data in the whole forecast domain over the period 19 January–29 February 2008 and given as functions of forecast length. The control forecast from the 3D-Var (red curve), the 3D-Var hybrid (green curve), the 4D-Var (blue curve) and the 4D-Var hybrid (pink curve) experiments are included. The curve marked CASES indicates the number of observed values for the verification. Forecasts have been run with 6th hourly lateral boundary conditions.

4D-Var that includes no condensation processes, for example. The differences between RMS verification scores between the 3D-Var hybrid and the standard 3D-Var are significant on the 95 % significance level for relative humidity at all levels below 300 hPa, while the differences between RMS verification scores between the standard 4D-Var and standard 3D-Var are significant on the 95 % significance level for relative humidity at 500 hPa only.

6.2.2 Application of lagged ensembles in hybrid assimilation

The relatively small impact of the 4D-Var hybrid as compared to the standard 4D-Var should not necessarily be considered as a disappointment but rather as a recognition of the strengths of the standard 4D-Var assimilation technique with its implicit full rank flow-dependent assimilation structure functions. One of our hypotheses is that one needs to *enrich* the ensemble used in our 4D-Var hybrid with ensemble variability in more directions representing possible short range forecast errors. One straightforward way is to increase the ensemble size, but this is not technically feasible at present considering available computing power. Another way is to introduce stochastic components in the nonlinear forecast model (Palmer and Williams, 2010) that is used to integrate the ensemble of model states forward in time in order to sample at the source of uncertainties, but at present our knowledge on such sources of uncertainties is too limited within the HIRLAM community to make any such model perturbations meaningful.

A fairly simple way to increase the size of the ensemble to be used for the hybrid assimilation is to try to apply some time lagging technique. In a first trial it was natural to try some initial time lagging by complementing the +3 h background forecast ensemble from the previous data assimilation cycle, used in 4D-Var hybrid, with the +9 h forecast ensemble from the next to the previous data assimilation cycle. In this way, the size of the ensemble applied in the 4D-Var hybrid was doubled from 20 to 40. It turned out, however, that forecast verification scores were not improved (results are not shown) by increasing the ensemble size in this way. We concluded that the ensemble for the hybrid assimilation was not enriched by adding a +9 h hour ensemble to the +3 h ensemble valid at the same time, the forecast perturbations from two such consecutive assimilation cycles are too similar, possibly because assimilation increments at 06:00 and 18:00 UTC do not provide much new information due to the reduced networks of conventional observations.

Next we tried a more radical change by introducing a valid time lagging. Our idea was that by lagging the valid time it would be possible to better correct for timing errors (and implicitly spatial phase errors). Thus, in addition to the +3 h background forecast valid at the start of the data assimilation window in 4D-Var hybrid, we added the +5 h background forecast valid 2 h into the data assimilation window. Although valid at different times, with a time difference of 2 h, we used these two ensembles to represent the flow-dependent background error covariance at the start of the assimilation window. This ad hoc trial turned out to be more successful. Most forecast verification scores (not shown) were slightly improved by adding the ensemble with the wrong valid time. The time series of the mean sea level pressure forecast verification scores over the Scandinavian verification domain revealed that forecasts for a few situations were improved by the additional ensemble component, in particular for the case 27 January 2008 12:00 UTC + 24 h the standard deviation verification scores were reduced by almost 50 %.

The difference between the mean sea level pressure forecasts produced with and without the valid time lagged ensemble for 27 January 12:00 UTC + 24 h are shown in Fig. 13

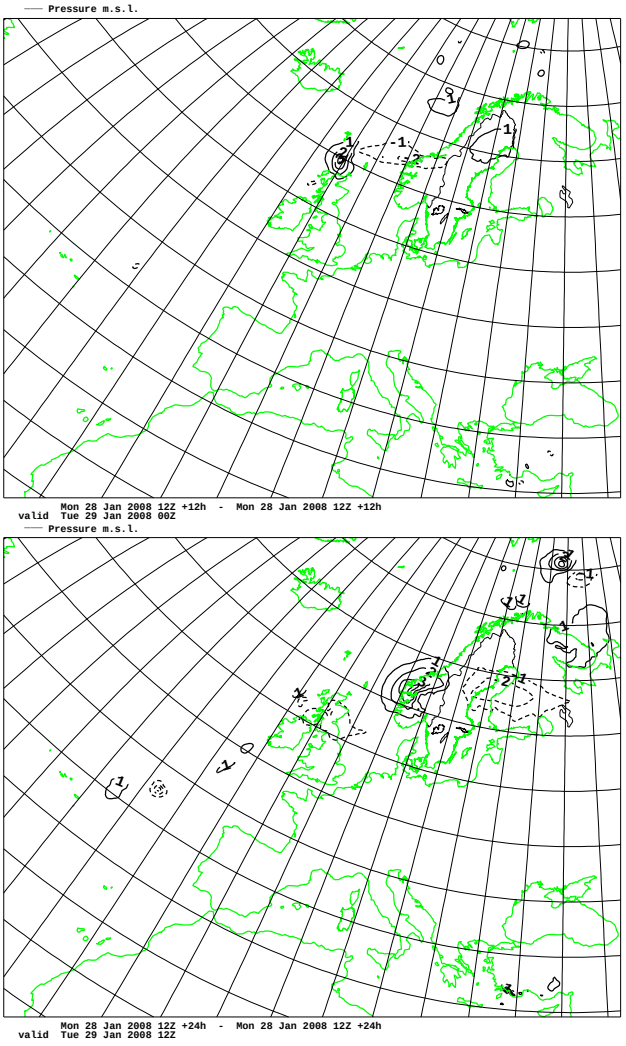

Fig. 13. Differences between mean sea level pressure forecasts from the 4dvar_hybrid1 and the 4dvar_hybrid2 experiments. 27 January 2008 +12 h (top panel) and +24 h (bottom panel). The difference between the two experiments is that 4dvar_hybrid2 uses an additional valid time lagged (+2 h) ensemble in the 4D-Var hybrid ensemble covariance. Isoline spacing 1 hPa.

(bottom panel) and the differences between the corresponding + 12 h forecasts are shown in Fig. 13 (top panel). Although it may be a random coincidence, these two consecutive forecast difference maps indicate a typical phase error in the southwest to northeast storm track from the Atlantic, over the British Isles towards Scandinavia. A trial to track these forecast differences back in time to explain initial data increment differences turned out to be too difficult due to too small assimilation increments being accumulated over several data assimilation cycles.

We may consider that this trial at least proves the concept of applying lagged valid time ensembles for hybrid variational ensemble data assimilation, when available computer

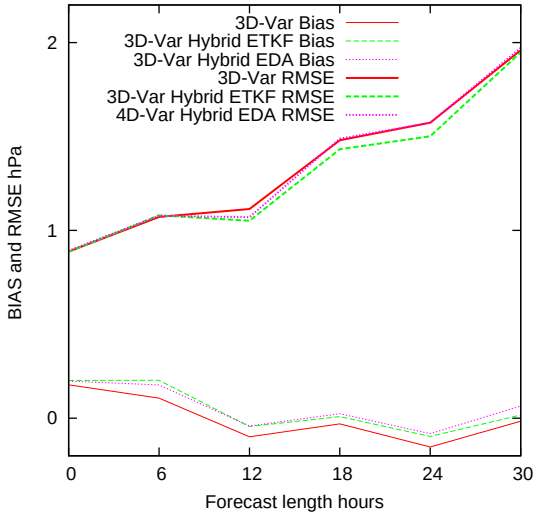

Fig. 14. Bias and standard deviation verification scores for mean sea level pressure forecasts over a Scandinavian domain averaged over the period 19 January–29 February 2008 and given as functions of forecast length. The control forecast from the 3D-Var (red full curve), the 3D-Var hybrid based on the ETKF ensemble (green dashed curve) and the 3D-Var hybrid based on the EDA ensemble (pink dotted curve) experiments are included. Forecasts have been run with 12th hourly lateral boundary conditions.

resources do not allow increase of the total ensemble size in the ensemble prediction system.

6.2.3 A comparison between EDA and ETKF ensembles for hybrid assimilation

Verification scores for forecasts from the standard 3D-Var, the 3D-Var hybrid based on ETKF ensemble perturbations and the 3D-Var hybrid based on EDA ensemble perturbations are included in Fig. 14 for mean sea level pressure forecasts over a Scandinavian domain verified against surface observations and in Fig. 15 for wind speed and relative humidity forecast profiles verified against radiosonde observations in the whole forecast domain. It may be concluded from the figures that also the 3D-Var hybrid based on an EDA ensemble provides improved forecast verification scores as compared with the standard 3D-Var, although the positive impact of 3D-Var with the EDA ensemble is slightly smaller than the positive impact with the ETKF ensemble. One may wonder whether the differences in performance between the two 3D-Var hybrid schemes is just a matter of tuning, for example, the inflation factors applied in the ensemble generation schemes, the magnitude of the observation perturbation or the scaling of the ensemble perturbations in the hybrid assimilation.

The differences between the ETKF based ensemble perturbations and the EDA based ensemble perturbations are further illustrated by examples of such perturbations in Fig. 16. Included in the figure are model level 28 wind

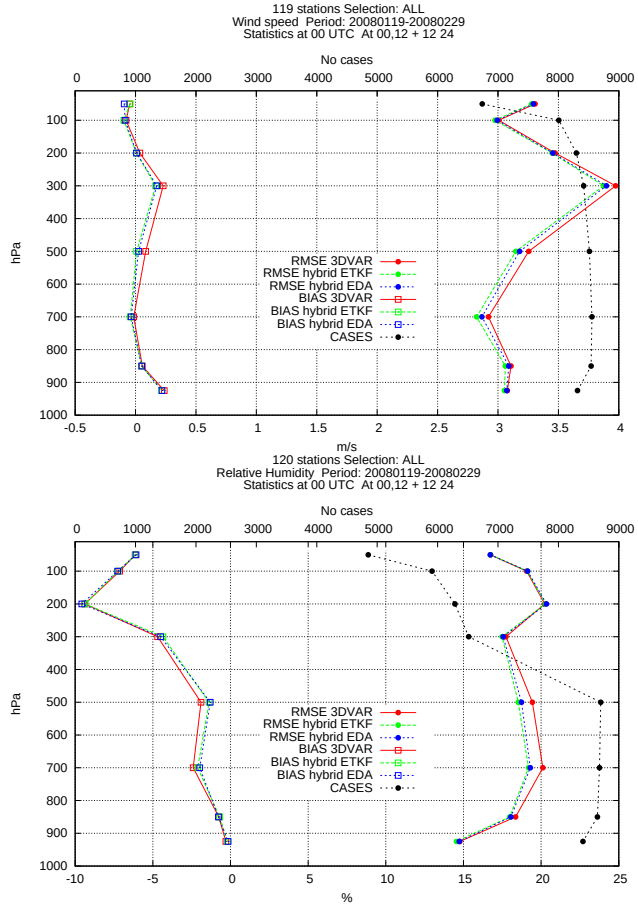

Fig. 15. Bias and standard deviation verification scores for wind speed (upper panel) and relative humidity (lower panel) profile forecasts as verified against radiosonde data in the whole forecast domain over the period 19 January–29 February 2008 and given as functions of forecast length. The control forecast from the 3D-Var (red curve), the 3D-Var hybrid based on the ETKF ensemble (green curve) and the 3D-Var hybrid based on the EDA ensemble (blue curve) experiments are included. The curve marked CASES indicates the number of observed values for the verification. Forecasts have been run with 12th hourly lateral boundary conditions.

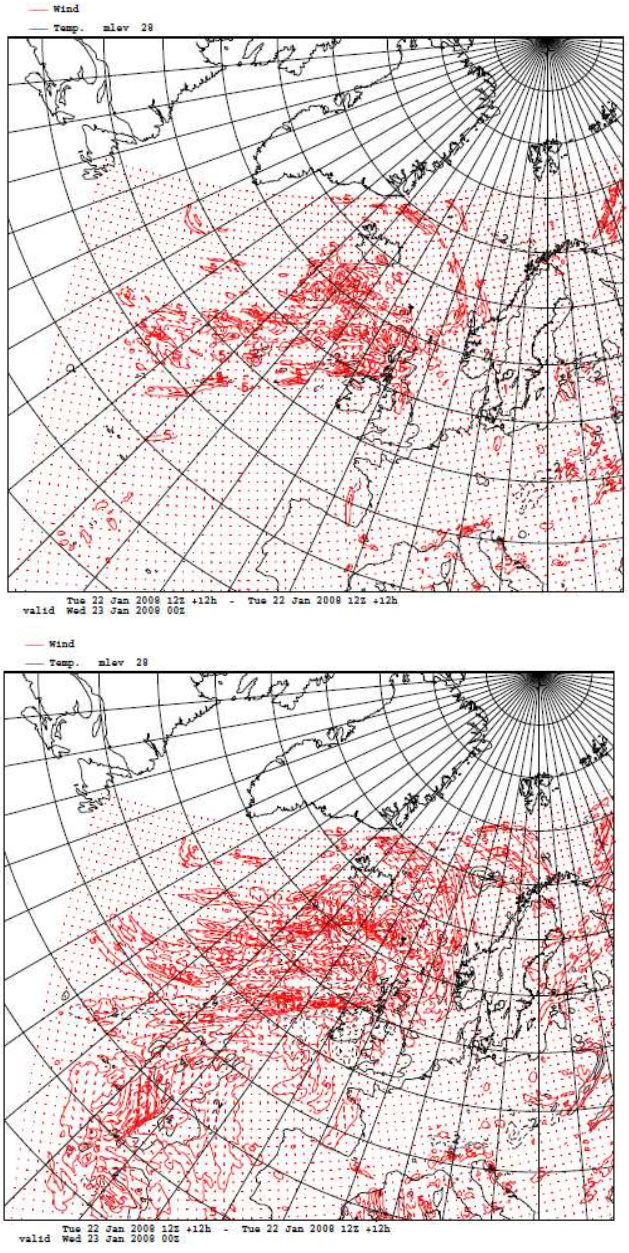

Fig. 16. Temperature and wind ensemble forecast perturbations at model level 28 for ensemble member 5, 22 January 2008 12:00 UTC + 12 h. ETKF based perturbations (upper panel) and EDA based perturbations (lower panel).

and temperature perturbations from ensemble member 5 for 22 January 2008 12:00 UTC + 12 h. Note that member 5 from the two experiments are driven by the same EuroTEPS lateral boundary conditions. We may notice that the ETKF based perturbations are dominated by dynamically coherent structures in the vicinity of an atmospheric front, while the EDA based perturbations include also slightly more noisy features, most likely originating from the perturbation of observations.

The different character of the EDA based ensemble perturbations is also confirmed by ensemble perturbation spectra in ensemble space calculated from differences between ensemble members and ensemble control in observation points. Such spectra for 22 January 2008 12:00 UTC + 6 h are included in Fig. 17. The spectrum for the EDA-based ensemble is significantly more flat than all the ETKF-based spectra, supporting the hypothesis that the EDA-based perturbations have less energy in the dynamically unstable structures. Furthermore, we may notice from the figure that the 4D-Var based perturbations have relatively larger variability in the first few eigenvectors of the ensemble space background error covariance matrix, as compared with the 3D-Var based perturbations. This is an indication of the strength

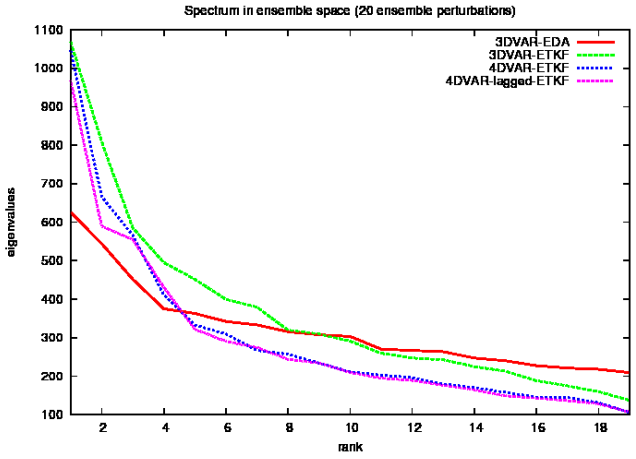

Fig. 17. Ensemble perturbation spectra in ensemble space calculated from differences between ensemble members and ensemble control in observation points. 22 January 2008 12:00 UTC + 6 h. 3D-Var hybrid with EDA perturbations (eda_hybrid1, red curve), 3D-Var hybrid with ETKF perturbations (3dvar_hybrid1, green curve), 4D-Var hybrid with ETKF perturbations (4dvar_hybrid1, blue curve) and 4D-Var hybrid with ETKF perturbations including also a lagged valid time ensemble (4dvar_hybrid2, pink curve).

of the 4D-Var assimilation algorithm to project the observed information (the innovations) on dynamically active features being selected and magnified through the integration of the tangent linear model during the assimilation as well as during the subsequent nonlinear model integration of the data assimilation cycles.

7 Concluding remarks

A hybrid variational ensemble data assimilation for the HIRLAM forecasting system has been developed and it has been validated with the emphasis to prove the concept of the hybrid assimilation as a true synthesis of variational and ensemble data assimilation techniques. Parallel data assimilation and forecast experiments have been carried out with different parameter settings for the hybrid scheme in addition to a comparison with the original 3D-Var and 4D-Var schemes. One version of the hybrid assimilation scheme, with equal weights assigned to the static (original 3D-Var) background error covariance and the ensemble based background error covariance, proved to provide improved forecast verification scores, as compared to 3D-Var over a short (8 day) period in August 2007. We also learned that the spectral density that constrains the localised weights applied to the different ensemble perturbations should have sufficient energy in larger scales, in order to preserve important structures provided by the ensemble and to prevent a too strong modification of these structures by averaging in the extended ensemble space.

The 3D-Var, the 3D-Var hybrid, the 4D-Var and the 4D-Var hybrid were compared in full-scale data assimilation and forecast experiments for a 6 weeks winter period, 17 January–29 February 2008. For the winter period, an additional tuning of the contribution of the ensemble perturbations to the assimilation increment was introduced in order to optimise the forecast performance. It turns out that 3D-Var hybrid and 4D-Var both significantly outperform the standard 3D-Var, while the improvement of 4D-Var hybrid over the standard 4D-Var is less significant. This is indeed a quite natural result, since already the standard 4D-Var by itself provides implicit flow-dependent assimilation structure functions. Clayton et al. (2013) reported on similar problems at the UK Met. Office to find improvements by 4D-Var hybrid over a standard 4D-Var for a global model. It was only after introduction of a vertical localisation (not yet implemented in HIRLAM) in the hybrid assimilation that the 4D-Var hybrid managed to outperform the standard 4D-Var.

We have also investigated the sensitivity of the performance of the hybrid assimilation to the applied ensemble generation technique. Thus by adding a +2 h lagged valid time ensemble to the standard ensemble valid at the start of the data assimilation window in the 4D-Var hybrid, it was possible to double the size of the ensemble applied in the 4D-Var hybrid. The motivation for this particular choice of ensemble time lagging was to try to improve the handling of timing errors (and implicitly spatial phase errors) in the data assimilation process. A slightly positive impact of this lagged ensemble approach certainly proves the concept and encourages us to continue similar investigations. Finally, we have also compared hybrid assimilation based on ETKF rescaling with hybrid assimilation based on ensemble perturbations generated by an Ensemble of Data Assimilations (EDA), including observation perturbations. Our first results indicate that the 3D-Var hybrid based on ETKF rescaling and the 3D-Var hybrid based on EDA perturbations provide comparable forecast quality in terms of forecast verification scores. The EDA based perturbations appear to include slightly more noisy spatial structures.

The results of this first validation of the hybrid data assimilation have encouraged us to continue the development and validation with regard to several aspects of its formulation. The horizontal correlation spectrum applied to the localised weights for the ensemble perturbations needs to be further examined and we should also investigate the need for a vertical localisation.

Furthermore, we have already made some progress in changing the 4D-Var hybrid formulation to utilise directly the ensemble of 4-D nonlinear model trajectories over the 4D-Var assimilation window in the observation operators in order to avoid the time integration of the tangent linear and adjoint models during the 4D-Var minimisation (4DEnVar, Liu et al., 2008, 2009). The first results of 4DEnVar indicate significantly improved humidity forecasts as compared to 4D-Var and 4D-Var Hybrid, confirming our speculations

above on the weaknesses of the TL and AD models of the HIRLAM 4D-Var to handle moist processes.

Acknowledgements. We would like to express our thanks to Dale Barker for stimulating discussions on the formulation of the Hybrid assimilation and to Kai Sattler for helping us with complicated scripting system for the HIRLAM EPS (Ensemble Prediction System). This research was partially funded by the eVITA programme of the Research Council of Norway, under contract 178894. This work was also supported by the Swedish National Space Board (Contract Dnr 105/08:3). The HIRLAM (HIgh Resolution Limited Area Model) project is a joint effort among the weather services in Denmark, Estonia, Finland, France, Iceland, Ireland, Lithuania, the Netherlands, Norway, Spain and Sweden for development of short range numerical weather prediction techniques. Three anonymous reviewers provided comments that made it possible to improve the manuscript.

Edited by: O. Talagrand
Reviewed by: L. Berre and two anonymous referees

References

Berre, L.: Estimation of synoptic and mesoscale forecast error covariances in a limited area model, Mon. Weather Rev., 128, 644–667, 2000.

Berre, L. and Desroziers, G.: Filtering of background error variances and correlations, Mon. Weather Rev., 138, 3693–3720, 2010.

Bishop, C. H., Etherton, B. J., and Majumdar, S. J.: Adaptive Sampling with the Ensemble Transform Kalman Filter, Part I: Theoretical Aspects, Mon. Weather Rev., 129, 420–436, 2001.

Bojarova, J., Gustafsson, N., Johansson, A., and Vignes, O.: The ETKF rescaling scheme in HIRLAM, Tellus A, 63, 385–401, 2011.

Buehner, M.: Ensemble-derived stationary and flow-dependent background-error covariances: Evaluation in a quasi-operational nwp setting, Q. J. Roy. Meteorol. Soc., 131, 1013–1043, 2005.

Buehner, M., Houtekamer, P., Charette, C., Mitchell, H., and He, B.: Intercomparison of variational data assimilation and the ensemble Kalman filter for global deterministic NWP, Part I: Description and single-observation experiments, Mon. Weather Rev., 138, 1550–1566, 2010a.

Buehner, M., Houtekamer, P., Charette, C., Mitchell, H., and He, B.: Intercomparison of variational data assimilation and the ensemble Kalman filter for global deterministic NWP, Part II: One-month experiments with real observations, Mon. Weather Rev., 138, 1567–1586, 2010b.

Clayton, A. M., Lorenc, A. C., and Barker, D. M.: Operational implementation of a hybrid ensemble/4D-Var global data assimilation at the Met Office, Q. J. Roy. Meteorol. Soc., 139, 1445–1461, 2013.

Courtier, P., Thepaut, J.-N., and Hollingsworth, A.: A strategy for operational implementation of 4D-Var, using an incremental approach, Q. J. Roy. Meteorol. Soc., 120, 1367–1387, 1994.

Cuxart, J., Bougeault, P., and Redelsperger, J.-L.: A turbulence scheme allowing for mesoscale and large-eddy simulations, Q. J. Roy. Meteorol. Soc., 126, 1-30, 2000.

Dee, D. P.: On-line estimation of error covariance parameters for atmospheric data assimilation, Mon. Weather Rev., 123, 1128-1145, 1995.

Durbin, J. and Koopman, S. J.: Monte Carlo maximum likelihood estimation of non-Gaussian state space model, Biometrika, 84, 669–684, 1997.

Evensen, G.: Sequential data assimilation with a nonlinear QG model using Monte Carlo methods to forecast error statistics, J. Geophys. Res., 99, 10143–10162, 1994.

Evensen, G.: Data Assimilation, the Ensemble Kalman Filter, Springer, Berlin, Heidelberg, 279 pp., 2007.

Fisher, M.: Background error covariance modelling, in: Proceedings of the ECMWF Workshop on Recent Developments in Data Assimilation for Atmosphere and Ocean, 8–12 September 2003, Reading, 97–123, 2003.

Frogner, I. L. and Iversen, T.: High-resolution limited area ensemble predictions based on low-resolution targeted singular vector, Q. J. Roy. Meteorol. Soc., 128, 1321–1341, 2002.

Gandin, L. S.: Objective analysis of meteorological fields, Leningrad Hydromet. Press, Leningrad, 963.

Gaspari, G. and Cohn, S. E.: Construction of correlation functions in two and three dimensions, Q. J. Roy. Meteorol. Soc., 125, 723–757, 1999.

Gauthier, P. and Thépaut, J.-N.: Impact of the digital filter as a weak constraint in the preoperational 4DVAR assimilation system of Météo-France, Mon. Weather Rev., 129, 2089–2102, 2001.

Gustafsson, N.: Use of a digital filter as weak constraint in variational data assimilation, Proceedings of a workshop on Variational assimilation, with special emphasis on three-dimensional aspects, ECMWF, Shinfield Park, Reading, UK, 1992.

Gustafsson, N.: Discussion on "4D-Var or EnKF", Tellus A, 59, 774–777, 2007.

Gustafsson, N. and Huang, X.-Y.: Sensitivity experiments with the spectral HIRLAM and its adjoint, Tellus A, 48, 501–517, 1996.

Gustafsson, N., Berre, L., Hörnquist, S., Huang, X.-Y., Lindskog, M., Navascués, B., Mogensen, K. S., and Thorsteinsson, S.: Three-dimensional variational data assimilation for a limited area model, Part I: General formulation and the background error constraint, Tellus A, 53, 425–446, 2001.

Gustafsson, N., Huang, X.-Y., Yang, X., Mogensen, K., Lindskog, M., Vignes, O., Wilhelmsson, T., and Thorsteinsson, S.: Four-dimensional variational data assimilation for a limited area model, Tellus A, 64, 14985, doi:10.3402/tellusa.v64i0.14985, 2012.

Hamill, T. M. and Snyder, C.: A hybrid ensemble Kalman filter-3D variational analysis scheme, Mon. Weather Rev., 128, 2905–2919, 2000.

Haugen, J. E. and Machenhauer, B.: A spectral limited-area model formulation with time-dependent boundary conditions applied to the shallow water equations, Mon. Weather Rev., 121, 2618–2630, 1993.

Houtekamer, P. L., Lefaivre, L., Derome, J., Ritchie, H., and Mitchell, H. L.: A System Simulation Approach to Ensemble Prediction, Mon. Weather Rev., 124, 1225–1242, 1996.

Kain, J. S.: The Kain-Fritsch convective parameterization: An update, J. Appl. Meteorol., 43, 170–181, 2004.

Kalman, R.: A new approach to linear filter and prediction theory, J. Basic. Eng., 82D, 35–45, 1960.

Kalman, R. and Bucy, R.: New results in linear filtering and prediction theory, J. Basic Eng., 83D, 95–108, 1961.

Kalnay, E., Li, H., Miyoshi, T., Yang, S., and Ballabrera-Poy, J.: 4D-Var or ensemble Kalman filter?, Tellus A, 59, 758–773, 2007.

Kepert, J. D.: Covariance localisation and balance in an Ensemble Kalman Filter, Q. J. Roy. Meteorol. Soc., 135, 1157–1176, 2009.

Lindskog, M., Gustafsson, N., Navascués, B., Mogensen, K. S., Huang, X.-Y., Yang, X., Andrae, U., Berre, L., Thorsteinsson, S., and Rantakokko, J.: Three-dimensional variational data assimilation for a limited area model, Part II: Observation handling and assimilation experiments, Tellus A, 53, 447–468, 2001.

Lindskog, M., Gustafsson, N., and Mogensen, K. S.: Representation of background error standard deviations in a limited area model dats assimilation system, Tellus A, 58, 430–444, 2006.

Liu, C., Xiao, Q., and Wang, B.: An ensemble-based four-dimensional variational data assimilation scheme, part i: Technical formulation and preliminary test, Mon. Weather Rev., 136, 3363–3373, 2008.

Liu, C., Xiao, Q., and Wang, B.: An ensemble-based four-dimensional variational data assimilation scheme, part ii: Observing System Simulation Experiments with advanced research WRF (ARW), Mon. Weather Rev., 137, 1687–1704, 2009.

Lorenc, A.: A global three-dimensional multivariate statistical interpolation scheme, Mon. Weather Rev., 109, 701–721, 1981.

Lorenc, A.: The potential of the ensemble Kalman filter for NWP – A comparison with 4D-Var, Q. J. Roy. Meteorol. Soc., 129, 3183–3203, 2003.

Noilhan, J. and Mahfouf, J.-F.: The ISBA land surface parameterization scheme, Global Planet. Change, 13, 145-1-59, 1996.

Ott, E., Hunt, B. R., Szunyogh, I., Zimin, A. V., Kostelich, E. J., Corazza, M., Kalnay, E., Patil, D. J., and Yorke, J. A.: A local ensemble Kalman filter for atmospheric data assimilation, Tellus A, 56, 415–428, 2004.

Palmer, T. and Williams, P.: Stochastic Physics and Climate Modelling, Cambridge University Press, 480 pp., 2010.

Pannekoucke, O., Berre, L., and Desroziers, G.: Filtering properties of wavelets for the local backgroubd error correlations. Q. J. Roy. Meteorol. Soc., 133, 363–379, 2007.

Papadakis, N., Mémin, E., Cuzol, A., and Gengembre, N.: Data assimilation with the weighted ensemble Kalman filter, Tellus A, 62A, 673–697, 2010.

Rasch, P. J. and Kristjánsson, J. E.: A comparison of the CCM3 model climate using diagnosed and predicted condensate parameterizations, J. Climate, 11, 1587–1614, 1998.

Savijärvi, H.: Fast radiation parameterization schemes for mesoscale and short-range forecast models, J. Appl. Meterol., 29, 437–447, 1990.

Tippett, M. K., Anderson, J. L., Bishop, C. H., Hamill, T. M., and Whitaker, J. S.: Ensemble Square Root Filters, Mon. Weather Rev., 131, 1485–1491, 2003.

Undén, P., Rontu, L., Järvinen, H., Lynch, P., Calvo, J., Cats, G., Cuxart, J., Eerola, K., Fortelius, C., Garcia-Moya, J. A., Jones, C., Lenderlink, G., McDonald, A., McGrath, R., Navascues, B., Woetman Nielsen, N., Odegaard, V., Rodriguez, E., Rummukainen, M., Rööm, R., Sattler, K., Hansen Sass, B., Savijärvi, H., Wichers Schreur, B., Sigg, R., The, H., and Tijm, A.: HIRLAM-5 Scientific Documentation, HIRLAM-5 project, c/o Per Undén, SMHI, Norrköping, Sweden, 2002.

van Leeuwen, P. J.: Particle filtering in geophysical systems, Mon. Weather Rev., 137, 4089–4114, 2009.

Wang, X., Bishop, C. H., and Julier, S. J.: Which is Better, an Ensemble of Positive- negative Paairs or a Centered Spherical Simplex Ensemble?, Mon. Weather Rev., 132, 1590–1605, 2004.

Wang, X., Snyder, C. and Hamill, T. M.: On the theoretical equivalence of differently proposed ensemble-3DVar hybrid analysis schemes, Mon. Weather Rev., 135, 222–227, 200.

Wang, X., Barker, D. M., Snyder, C., and Hamill, T. M.: A Hybrid ETKF-3DVar Data Assimilation Scheme for the WRF Model, Part I: Observing System Simulation Experiment, Mon. Weather Rev., 136, 5116–5131, 2008a.

Wang, X., Barker, D. M., Snyder, C., and Hamill, T. M.: A Hybrid ETKF-3DVar Data Assimilation Scheme for the WRF Model, Part I: Real Observation Experiments., Mon. Weather Rev., 136, 5132–5147, 2008b.

Wang, X., Hamill, T. M., Whitaker, J. S., and Bishop, C. H.: A Comparison of the Hybrid and EnSRF Analysis Schemes in the Presence of the Model Errors due to Unresolved Scales, Mon. Weather Rev., 137, 3219–3232, 2009.

Zhang, M. and Zhang, F.: E4DVar: Coupling an Ensemble Kalman Filter with Four-Dimensional Variational Data Assimilation in a Limited-Area Weather Prediction Model, Mon. Weather Rev., 140, 587–600, 2012.